Ecological Indicators 155 (2023) 110979

Contents lists available at ScienceDirect

Ecological Indicators

journal homepage: www.elsevier.com/locate/ecolind

Original Articles

Modeling the influence of daily temperature and precipitation extreme indices on vegetation dynamics in Katsina State using statistical downscaling model (SDM)

Mohammad Hadi Ahmad [a,b], Ahmed Abubakar [c], Mohd Yusoff Ishak [c], Samir Shehu Danhassan [d], Zhang Jiahua [d], Juha M. Alatalo [e,*]

[a] Department of Geography and Environmental Management, Ahmadu Bello University Zaria, Nigeria
[b] Space Applications Department, Zonal Advanced Space Technology Applications Laboratory National Space Research and Development Agency, Nigeria
[c] Faculty of Forestry and Environment, Universiti Putra Malaysia, Serdang, Selangor 43400, Malaysia
[d] College of Earth and Planetary Sciences, University of Chinese Academy of Sciences, Beijing 100049, China
[e] Environmental Science Center, Qatar University, Doha, Qatar

ARTICLE INFO

Keywords:
Vegetation
Precipitation
Maximum temperature
Minimum temperature

ABSTRACT

Climate change significantly impacts local, regional, and global vegetation changes. These changes have continued to threaten ecosystems, especially in dryland areas where moisture is scarce, and the livelihoods of rural communities are at risk because of such changes, as well as their capacity to provide outputs and sustain the livelihoods of rural communities. This study aims to derive a simulation model of vegetation conditions concerning daily temperature and extreme precipitation indices in Katsina State, Nigeria. This study uses remote sensing and Geographic Information System (GIS)-based analysis, time series analysis of precipitation, maximum and minimum temperature, and twenty-four indices defined by the Expert Team on Climate Change Detection to evaluate the influence of Temp and precipitation extreme indices on vegetation dynamics/NDVI. The results indicate that the statistical downscaling model (SDSM) is performing satisfactorily in predicting maximum and minimum temperatures, along with precipitation, for the time horizon of the simulation. Mean precipitation of 1.98 mm (RCP2.6), 2.03 mm (RCP4.5), and 2.07 mm (RCP8.5) was revealed in the study area. Tmax and Tmin were projected under low emissions at 20.1 ^{0}C and 14.25 ^{0}C (RCP2.6), 20.13 °C and 14.26 ^{0}C (RCP4.5), and 20.15 ^{0}C and 14.27 ^{0}C (RCP8.5) respectively. All the scenarios present increasing minimum and maximum temperatures and decreasing precipitation, except for RCP8.5, which predicted a more adverse trend. However, in Katsina State, the Normalized Difference Vegetation Index (NDVI), precipitation, Tmax, and Tmin, extreme temperature and precipitation indices, and drought indices successfully demonstrated spatial and temporal variability.

1. Introduction

The influence of climatic variability on tropical vegetation holds great importance at the global, regional, and local levels due to its abundant biodiversity and its ability to impact the cycles of carbon, water, and nutrients (Jansson and Hofmockel, 2020). Understanding the effects of climate change and vegetation restoration on ecosystem services is crucial for implementing sustainable ecosystem management practices. The preservation of vegetation has a key role in attaining sustainable development at a global level (Ma et al., 2021). The presence of vegetation is crucial in shaping the carbon and climate systems on terrestrial surfaces, impacting ecosystem service delivery (Quijas et al., 2010; Buytaert et al., 2011). The development and dispersion of plant life are significantly affected by a combination of human activities and natural phenomena (Cao et al., 2014). Consequently, the system elements demonstrate seasonal and successional fluctuations, leading to a wide range of reactions and feedback mechanisms among different species and ecosystems (Weiskopf et al., 2020). Cao et al. (2014) propose that the climate of a specific region can be classified as either macroclimatic or microclimatic, depending on the perspective adopted. Prior studies have demonstrated a significant association between climate variability, which refers to fluctuations in climate conditions over a

* Corresponding author.
E-mail address: jalatalo@qu.edu.qa (J.M. Alatalo).

https://doi.org/10.1016/j.ecolind.2023.110979
Received 27 March 2023; Received in revised form 18 September 2023; Accepted 19 September 2023
Available online 7 October 2023
1470-160X/© 2023 The Author(s). Published by Elsevier Ltd. This is an open access article under the CC BY license (http://creativecommons.org/licenses/by/4.0/).

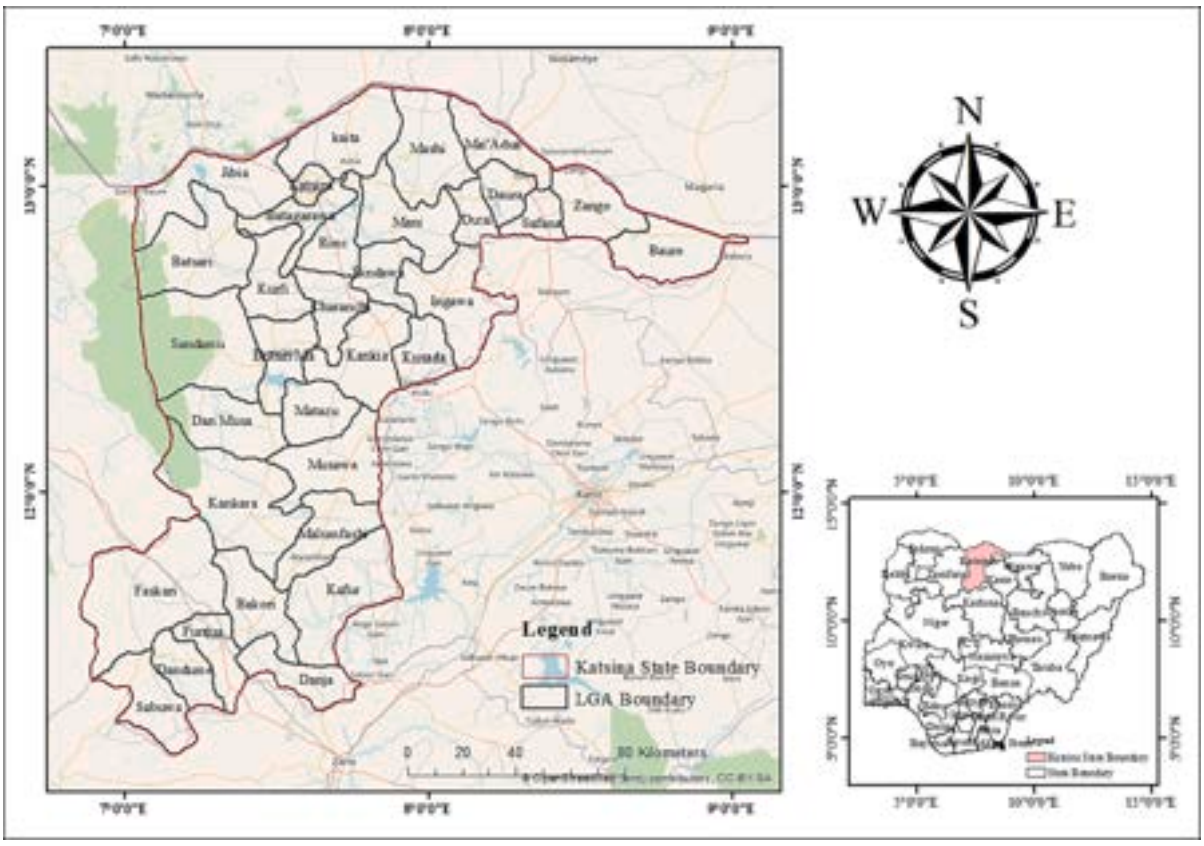

Fig. 1. Map of the study area.

specific timeframe, and the dynamics of vegetation growth and development (Cao et al., 2014; Thornton et al., 2014). The issue of climate change has become a prominent aspect of the present-day difficulties faced in terms of global food security and human health (Hanjra and Qureshi, 2010).

Local communities and resource managers require an awareness of variability and climate change to adjust plans for greater fluctuation brought on by global climate change (Twomlow et al., 2008; O'Connell, 2017). Plant biochemical and biophysical processes influence climate change (Perugini et al., 2017). Several examples of biophysical factors include vegetation characteristics that impact latent heat distribution, emissivity, and albedo (Cao et al., 2015).

According to climate change forecasts, Africa will see severe climate and vegetation changes (Scheiter and Higgins, 2009; Scheiter and Higgins, 2009; Scheiter and Higgins, 2009; Anav and Mariotti, 2011; Sarr, 2012). Drought is expected to continue to impact the vegetation along the Guinea Coast and the Sahel in West Africa, causing significant changes (Mehboob et al., 2020). In West Africa and Nigeria, rainfall and temperature are the most influencing elements of vegetation change (Abiodun et al., 2012; Sinare and Gordon, 2015). Climate variability has negatively affected vegetation through recurrences of drought (Bouriaud et al., 2005). There have been recent reports of tree dieback caused by drought in numerous forests around the world (Galiano et al., 2010). This affects the structure and function of the ecosystem (Galiano et al., 2010). Due to a prolonged desiccation period that started in the late 1960 s and continued into the 1990 s, the West African Sahel, particularly the drylands of Nigeria, has been the subject of much drought research (Hulme, 2001; Brooks, 2004; Adejuwon and Dada, 2021). However, the bulk of drought studies (Giannini and Kaplan, 2019; Carré et al., 2019; Biasutti, 2019; Carré et al., 2019; Ibrahim et al., 2020) have focused on drought occurrence, causes, effects, and farmers' adaptation. Other studies in Katsina focused on temperature and rainfall variability (Adejuwon and Dada, 2021; Dogonyaro et al., 2022; Ibrahim and Abdullahi, 2022; Ogunsola et al., 2022; Saleh, 2020).

Vegetation indices and ecological interactions between woody and herbaceous plant species in Nigeria show that the vegetation's structure, distribution, and variety have changed due to climate change and population fluctuations (Obioha, 2008; Obioha, 2009). Nigeria, as a country, loses more than 350,000–400,000 ha of vegetation annually due to human activities (Akpu et al., 2017). Furthermore, logging is one of Nigeria's most common forest disturbances (Okon, 2018). For instance, wood is a significant energy source in Nigeria (Adamu et al., 2020). In addition, grazing is a principal cause of tropical vegetation degradation (Alaanuloluwa Ikhuoso et al., 2020). In general, increasing population, expansion of agriculture, unsustainable forest use, and urbanization are the causes of vegetation change in tropical regions (Duveiller et al., 2008).

To plan for the future, we must comprehend how the climate changes, especially in vulnerable regions like Katsina State. Threats like declining vegetation and climate change represent complex challenges, as does fluctuation in the climate. Policymakers must know climate change's present and future implications and variability to lessen its effects in the studied region. By examining concerns relating to climate change and variability in Katsina State, Nigeria, this study adds to the body of literature. Geospatial technologies are an effective tool for researching the changes in the world's vegetation (Langat et al., 2019). Using a statistical downscaling model, the present study's goal is to evaluate the impact of daily temperature and extreme precipitation indices on the vegetation dynamics in Katsina state.

One major challenge in understanding climate change's impact on vegetation dynamics is the need for accurate and high-resolution climate data at the local level. This study aims to address this challenge by using a statistical downscaling model (SDM) to model the influence of daily temperature and extreme precipitation indices on vegetation dynamics in Katsina State, Nigeria. Katsina State is one of the most populous states in Nigeria and is known for its agricultural activities. The state's

Table 1
Data Types and Sources.

S/N	Data Type	Source
1	Meteorological data: Rainfall, Maximum and Minimum Temperature	ERA5, Historical CMIP5, and NiMet 1982 to 2021 (40 years)
2	Population Data	National Bureau of Statistics, Nigeria, website (https://www.nigerianstat.gov.ng/download)
3	Digital Elevation Model (DEM)	The SRTM DEM website https://www.diva-gis.org/gdata
4	Photographs	Field Survey
5	Works of literature	Journals, textbooks, internet materials, conference papers, newspapers, unpublished dissertations, and thesis
6	Administrative map of Nigeria	DIVA GIS
7	NOAA Global Inventory Modelling and Mapping Studies (GIMMS) AVHRR Normalized Difference Vegetation Index (NDVI) product (1982–1999)	(https://www.glcf.umd.edu/data/gimms/) to examine a long-time series of vegetation condition
8	Moderate Resolution Imaging Spectroradiometer (MODIS) MOD13 NDVI (2000–2021)	Land Processes Distributed Active Archive Centre (LP DAAC), NASA

Source: Author's Compilation, 2022.

vegetation, which is mainly made up of grasslands, savannas, and woodlands, is crucial to the livelihoods of the people living in the state (Ibrahim et al., 2022). However, the state has experienced changes in its temperature and precipitation patterns in recent years, which have affected its vegetation.

The study will use the SDM to downscale the global climate data to the local level, allowing for modeling the impact of daily temperature and precipitation extreme indices on vegetation dynamics. The results of this study will be crucial in informing policymakers and stakeholders in Katsina State on the impact of climate change on vegetation and the need for appropriate measures to mitigate its effects. Furthermore, the study's findings will contribute to the body of knowledge on the impact of climate change on vegetation dynamics and the use of SDM in modeling such effects.

2. Materials and methods

2.1. The study area

Katsina State is located in Northwestern Nigeria, between latitudes 11^0 07′ 49″ and 13^0 22′ 57″ north of the equator and longitudes 6^0 52′ 03″ and 9^0 09′ 02″ east of the Greenwich meridian" (see Fig. 1). As stated by the National Population Commission (2006), Katsina state has an estimated population of 5,792,578 people and a total area of around 23,938 square kilometers (Ahmadu et al., 2022). The Sahel, Sudan, and Northern Guinea Savanna are three of the state's agroecological zones. The semi-arid steppe types are classified as AW and BS and have a tropical wet and dry climate (Umar et al., 2021). Katsina state experiences temperatures between 29 ^{0}C and 31 ^{0}C and 350–1000 mm of annual rainfall (Idris et al., 2019; Alemaka et al., 2021). High interannual variability in spatial and temporal characteristics of the zone's rainfall pattern regularly results in severe and extensive droughts (Oladipo, 1993; Okorie, 2003).

The region has four distinct seasons, with February through May being the hottest. The rainy season lasts from April to October, characterized by a southwesterly predominating wind (Ohunakin et al., 2011). The dry season lasts from November to March, when the Harmattan, a Saharan breeze, dominates the wind (Umar, 2016). Although the dry northern air does not bring rain between November and February, the harmattan dust it delivers is deposited and replenishes soil nutrients. There isn't much cold air at night, but dust flows throughout the day (Ahmad and Daura, 2019). The harvesting season, or Cool Dry Season (Kaka), lasts from October to November and sees less than 8 % of the yearly rainfall, while the rainy or Damina season, lasting from June to October, sees over 90 % of the annual rainfall (Ahmad and Daura, 2019). Fig. 1 displays a map outlining the geographical extent of the study area.

2.2. Type and sources of data

Multiple data types and sources were used to accomplish this study's goal. The data type and sources for this investigation are shown in Table 1.

2.3. Data processing

GIMMS NDVI data are utilized in this study. Aerosols, the solar zenith angle, and orbital drift were all considered during the preprocessing of this data. All satellite-based data utilized in this work are adjusted to assess the impact of noise before data analysis. The global

Table 2
Description of the selected predictors for modeling the influence of extreme indices on vegetation.

S/NO	Predictor	Reasons for Selection
1	ncepmslpgl.dat	Mean Sea Level Pressure data can influence rainfall patterns, as areas of high and low pressure often correlate with weather systems affecting precipitation. This can also affect temperature by influencing air pressure, which in turn impacts temperature patterns.
2	ncepp1_vgl.dat	This variable, likely representing wind patterns in the upper atmosphere, can impact the movement and distribution of moisture, which is crucial for rainfall and temperature modeling.
3	ncepp1_ugl.dat	Wind patterns in the lower atmosphere can also significantly influence rainfall, making this variable relevant for modeling precipitation.
4	ncepp500gl.dat	Data related to atmospheric conditions at the 500mb level can provide insights into the dynamics that influence rainfall patterns at different altitudes in the atmosphere.
5	ncepp850gl.dat	Atmospheric conditions at the 850mb level can affect temperature, humidity, and air stability, all of which play roles in determining rainfall and temperature patterns.
6	ncepshumgl.dat	Humidity levels in the atmosphere can influence maximum and minimum temperature as high humidity tends to moderate temperature extremes.
7	ncepp5_zgl.dat	This variable, likely representing geopotential height, can help understand temperature patterns in the upper atmosphere and their impact on surface temperatures.
8	nceps500gl.dat	Conditions at the 500mb level are indicative of atmospheric dynamics that affect temperature, making this variable relevant for temperature modeling.
9	nceptempgl.dat	Surface temperature data is essential for modeling maximum and minimum temperatures, as it directly represents the variable of interest.

GIMMS NDVI dataset was initially loaded into remote sensing software to stack the 696 bi-monthly NDVI composites before image pre-processing. Following a reliability analysis of the data, a similar procedure was carried out for the MODIS NDVI datasets utilized in this work. The GIMMS-NDVI dataset is offered in global projection. Hence, it is necessary to re-project it to Universal Transverse Mercator (UTM). Additionally, subset images of the research area were trimmed from the datasets depending on the Katsina state administrative boundary. The monthly datasets were all re-projected. The two primary pre-processing phases were completed in IDRISI and R programming, followed by the evaluation of the intra-annual and seasonal trend analysis. The IDRISI pre-processing procedures apply to the entire study region or the satellite imagery that covers the study area. Datasets for Katsina state were cut from the GIMMS and MODIS NDVI images (Dagnachew et al., 2020). The purpose of doing this is to lessen noise or any other disturbance brought on by atmospheric effects.

2.4. Data analysis

Time series data of daily rainfall, maximum and minimum temperature spanning from 1982 to 2021 were acquired from the Nigerian Meteorological Agency (NiMet). NiMet, a government organization responsible for nationwide weather stations, provided the data and metadata for the study area. Outlier and homogeneity tests were conducted on the maximum and minimum temperature and rainfall data to ensure data quality. These tests helped identify and address any anomalies or inconsistencies in the dataset.

In addition to the NiMet data, the ERA5 dataset was obtained from the Copernicus Climate Change Service website (https://cds.climate.copernicus.eu). ERA5 is a fifth-generation ECMWF reanalysis dataset that provides comprehensive global climate and weather information for the past 4 to 7 decades. The dataset offers daily updates and has a spatial resolution of 0.25^0 grid.

Furthermore, Global Climate Model-derived predictors were sourced from a Canadian website (https://climate-scenarios.canada.ca/?page=sdi-cmip5intro). These predictors (see Table 2), derived from climate models, provide additional variables that can be used to enhance the analysis and better understand the influences on vegetation dynamics.

The selection of these predictors was based on their significance in the modeling of extreme indices, such as rainfall, maximum temperature, and lowest temperature, as well as their potential impact on vegetation dynamics. The selected variables comprise a diverse set of atmospheric and climatic circumstances that have the potential to greatly influence the variables of interest. This makes them well-suited for examination within the framework of vegetation modeling.

By utilizing the collected data from NiMet, the ERA5 dataset, and Global Climate Model-derived predictors, the data analysis aims to examine and model the impact of climatic variability within the study area between the years 1982 and 2021. The analysis will help uncover relationships between daily temperature and precipitation extreme indices and vegetation dynamics in the study area.

Normality Test.

The Anderson-Darling (A-D) statistic was then used to assess the data for normality, defined as:

$$A_n^2 = \int_{-\infty}^{\infty} |F_n(x) - F(x)|^2 \psi(x) f(x) d(x)$$

Where:

$$\psi(x) = n/F(x)\{1 - F(x)\}$$

n = Total number of data points;
F(x) = distribution function of the fitted distribution;
f(x) = density function of the fitted distribution;

Table 3
List of the 26 predictor filenames and their corresponding variable names.

S/N	Predictor Filenames	Variable names
1	ncepmslpgl.dat	Mean sea level pressure
2	ncepp1_fgl.dat	1000 hPa Wind speed
3	ncepp1_ugl.dat	1000 hPa Zonal wind component
4	ncepp1_vgl.dat	1000 hPa Meridional wind component
5	ncepp1_zgl.dat	1000 hPa Relative vorticity of true wind
6	ncepp1thgl.dat	1000 hPa Wind direction
7	ncepp1zhgl.dat	1000 hPa Divergence of true wind
8	ncepp500gl.dat	500 hPa Geopotential
9	ncepp5_fgl.dat	500 hPa Wind speed
10	ncepp5_ugl.dat	500 hPa Zonal wind component
11	ncepp5_vgl.dat	500 hPa Meridional wind component
12	ncepp5_zgl.dat	500 hPa Relative vorticity of true wind
13	ncepp5thgl.dat	500 hPa Wind direction
14	ncepp5zhgl.dat	500 hPa Divergence of true wind
15	ncepp850gl.dat	850 hPa Geopotential
16	ncepp8_fgl.dat	850 hPa Wind speed
17	ncepp8_ugl.dat	850 hPa Zonal wind component
18	ncepp8_vgl.dat	850 hPa Meridional wind component
19	ncepp8_zgl.dat	850 hPa Relative vorticity of true wind
20	ncepp8thgl.dat	850 hPa Wind direction
21	ncepp8zhgl.dat	850 hPa Divergence of true wind
22	ncepprcpgl.dat	Total precipitation
23	nceps500gl.dat	500 hPa Specific humidity
24	nceps850gl.dat	850 hPa Specific humidity
25	ncepshumgl.dat	1000 hPa Specific humidity
26	nceptempgl.dat	Air temperature at 2 *m*

$$F_n = \frac{i}{n}$$

i = the cumulative rank of the data point.

As a result, the A-D statistic is often a more relevant measure of fit than other statistics, such as the K-S statistic, especially when giving equal weight to fitting a distribution at the tails and the main body is crucial. The following theories are developed using the Anderson-Darling test for normality:

H_0 Data is from a normally distributed population;

H_1: Data are not from a normally distributed population;

The Anderson-Darling test's p-value determines the probability that the data are from a regularly distributed population. If the distribution fits the data, the related p-value was higher than the selected alpha level, and the A-D statistic was modest (0.05 and 0.10). Missing values are checked to see if the data is complete before deciding whether more analysis is required. WMO guidelines state that it is not advised to fill in more than 10 % of the missing data (WMO, 2017). As a result, we apply ordinary least squares (OLS) techniques to complete the climatic variable's missing data (Helsel and Hirsch, 1992). They are, therefore, utilized to ascertain the degree of climatic variability in the research area.

However, to ensure data consistency and comparability, the combined station data and ERA5 data were subjected to homogenization using the adapted Caussinus-Mestre algorithm for homogenizing networks of temperature series (ACMANT) method. This method, as described by Adeyeri et al. (2022) and Mamara et al. (2013), automatically detects breakpoints in the climatic data series by considering variables such as variable type and temporal resolution specific to the study region. The application of ACMANT enhances the accuracy of trend analysis, spatial coherence, and climatic pattern consistency (Adeyeri et al., 2022; Mamara et al., 2013). Notably, ACMANT has proven effective in homogenizing climate series by utilizing bivariate techniques to identify shifts in series mean.

SDM.

This model used multilinear regression to establish relationships between the 26 predictors of the National Centre of Environmental Prediction (NCEP) reanalysis data (Table 3), covering the period of 1961–2000. These predictors were employed in the Statistical Down Scaling Model (SDSM) to analyze and calibrate the connections between

Table 4
List of ETCCDI/Expert Team on Sector-Specific Climate Indices (ET-SCI) investigated in this study.

Element	Short name	Long name	Definition	Plain language description	Units	Time scale	Sector (s)
Precipitation Indices	CDD	Consecutive Dry Days	Maximum number of consecutive dry days (when PR < 1.0 mm)	Longest dry spell	days	Mon/ Ann	H, AFS, WRH
	CWD	Consecutive Wet Days	The maximum annual number of consecutive wet days (when PR >= 1.0 mm)	The longest wet spell	days	Ann	
	PRCPTOT	Annual total wet-day PR	Sum of daily PR >= 1.0 mm	Total wet-day rainfall	mm	Mon/ Ann	AFS, WRH
	R10mm	Number of heavy rain days	Number of days when PR >= 10 mm	Days when rainfall is at least 10 mm	days	Mon/ Ann	
	R20mm	Number of very heavy rain days	Number of days when PR >= 20 mm	Days when rainfall is at least 20 mm	days	Mon/ Ann	AFS, WRH
	R95p	Total annual PR from heavy rain days	The annual sum of daily PR > 95th percentile	Amount of rainfall from very wet days	mm	Ann	
	R99p	Total annual PR from very heavy rain days	The annual sum of daily PR > 99th percentile	Amount of rainfall from extremely wet days	mm	Ann	
	Rx1day	Max 1-day PR	Maximum 1-day PR total	The maximum amount of rain that falls in one day	mm	Mon/ Ann	
	Rx5day	Max 5-day PR	Maximum 5-day PR total	The maximum amount of rain that falls in five consecutive days	mm	Mon/ Ann	
	SDII	Daily PR intensity	Annual total PR divided by the number of wet days (when total PR >= 1.0 mm)	Average daily wet-day rainfall intensity	mm/ day	Ann	
Temperature Indices	DTR	Daily Temperature Range	Mean difference between daily TX and daily TN	The average range of maximum and minimum temperature	^{0}C	Mon/ Ann	
	GSL	Growing Season Length	The annual number of days between the first occurrence of 6 consecutive days with TM > 5 ^{0}C and the first occurrence of 6 consecutive days with TM < 5 ^{0}C	Length of time in which plants can grow	days	Ann	AFS
	CSDI	Cold spell duration indicator	The annual number of days contributing to events where 6 or more consecutive days experience TN < 10th percentile	Number of days contributing to a cold period (where the period has to be at least 6 days long)	days	Ann	H, AFS
	SU	Summer days	Number of days when TX > 25 ^{0}C	Days when the maximum temperature exceeds 25 °C	days	Mon/ Ann	H
	TN10p	Amount of cold nights	Percentage of days when TN < 10th percentile	Fraction of days with cold nighttime temperatures	%	Ann	
	TN90p	Amount of warm nights	Percentage of days when TN > 90th percentile	Fraction of days with warm nighttime temperatures	%	Ann	
	TNn	Min TN	Coldest daily TN	Coldest night	^{0}C	Mon/ Ann	AFS
	TNx	Max TN	Warmest daily TN	Hottest night	^{0}C	Mon/ Ann	
	TR	Tropical nights	Number of days when TN > 20 ^{0}C	Days when the minimum temperature exceeds 20 °C	days	Mon/ Ann	H, AFS
	TX10p	Amount of cool days	Percentage of days when TX < 10th percentile	Fraction of days with cool daytime temperatures	%	Ann	
	TX90p	Amount of hot days	Percentage of days when TX > 90th percentile	Fraction of days with hot daytime temperatures	%	Ann	
	TXn	Min TX	Coldest daily TX	Coldest day	^{0}C	Mon/ Ann	
	TXx	Max TX	Warmest daily TX	Hottest day	^{0}C	Mon/ Ann	AFS
	WSDI	Warm spell duration indicator	The annual number of days contributing to events where 6 or more consecutive days experience TX > 90th percentile	Number of days contributing to a warm period (where the period has to be at least 6 days long)	days	Ann	H, AFS, WRH
Drought Indices	SPEI	Standardized Precipitation Evapotranspiration Index	The measure of "drought" using the Standardised Precipitation Evapotranspiration Index on time scales of 3, 6, and 12 months. See Vicente-Serrano et al. (2010) for details. Calculated using the SPEI R package	A drought measure specified using precipitation and evaporation	unitless	Custom	H, AFS, WRH
	SPI	Standardized Precipitation Index	The measure of "drought" using the Standardised Precipitation Index on time scales of 3, 6, and 12 months. See McKee et al., (1993) and the WMO SPI User guide WMO (2012) for details. Calculated using the SPEI R package.	A drought measure specified as a precipitation deficit	unitless	Custom	H, AFS, WRH

Source: Adapted and Modified from Zang and Yang (2006).
NOTE: "Daily Minimum Temperature (TN), Daily Maximum Temperature (TX), and Daily Precipitation (PR), Daily Mean Temperature (TM) are calculated from TM = (TX + TN)/2. Diurnal Temperature Range (DTR) is calculated from DTR = TX – TN" (Zang and Yang, 2006). Indices are computed at both yearly (Ann) and monthly (Mon) temporal resolutions. The ET-SCI, in collaboration with sector representatives, has identified the relevant sectors for each indicator. These sectors include Health (H), Agriculture and Food Security (AFS), and Water Resources and Hydrology (WRH). Certain indexes have not undergone assessment in relation to particular sectors.

predictors and predictands. The daily predictors from the Canadian Earth System Model (CanESM2) of the CMIP5 project were utilized, considering the emissions from the RCP26, RCP45, and RCP28.5 scenarios. These datasets were processed for the SDSM to evaluate future climate variability.

The selection of these 26 GCM predictors was based on their relevance to several meteorological and climatic elements that have a substantial influence on extreme indices such as rainfall, temperature, and subsequently, vegetation dynamics. Together, these variables offer a broad range of factors that can be utilized to describe the intricate connections between climatic patterns and vegetation.

In order to understand the fluctuations in extreme climatic indices within the study area, the relationship between climate change, bias correction, and vegetation can be explored through the Statistical Downscaling Model (SDSM). Climatic variables serve as independent variables in the vegetation model to determine their correlation. The SDSM, originally developed by Wilby et al. (2002), integrates the Stochastic Weather Generator (SWG) and Multiple Linear Regression (MLR) techniques. Correlation analysis was employed to select GCM variables for downscaling rainfall, maximum temperature, and minimum temperature. A correlation value equal to or greater than 0.5 at a significance level of 0.05 was used as the criterion for variable retention.

The following GCM variables were selected for modeling rainfall: ncepmslpgl.dat, ncepp1_vgl.dat, ncepp1_ugl.dat, ncepp500gl, and ncepp850gl.dat. For maximum temperature, the chosen variables were ncepmslpgl.dat, ncepshumgl.dat, ncepp5_zgl.dat, nceps500gl.dat, and nceptempgl.dat. Similarly, for modeling minimum temperature, the selected variables were ncepp5_zgl.dat, ncepp1_vgl.dat, nceps850gl.dat, ncep-shumgl.dat, and nceptempgl,dat. MLR establishes statistical and empirical links between NCEP predictors and predictions during the predictor screening phase. The calibration process of SDSM generates regression parameters based on these links (Al-Mukhtar and Qasim, 2019).

To ensure validation, time series were used as a standard, following the approach of previous studies. These time series and NCEP and GCM predictors were employed to construct a maximum of 100 daily time series, closely corresponding to observed data (Wilby et al., 2002).

The Statistical Downscaling Model (SDSM) utilized in this study combines a stochastic weather generator and a regression algorithm, as introduced by Wilby et al. (2002). It assists users in selecting the most suitable large-scale climatic variables, known as predictors, by evaluating the variability in climate at a specific site or catchment scale. These predictors are then used to establish statistical relationships with daily observed data. Furthermore, these relationships are applied to generate daily weather data for future periods, using the Global Climate Models (GCMs) predictors, as shown by Tao et al. (2015).

For this analysis, the baseline period from 1961 to 1990 was selected, as it is widely employed as the climatic normal period in various climate studies globally (Huang, et al., 2011; Rashid, and Mukand, 2014). Following successful validation using graphical and skill score (R^2) techniques and subsequent bias correction using MBCn, daily time series data of climate variables were generated for three future periods: RCP26, RCP45, and RCP28.5, derived from the CanESM2 model.

Bias correction.

To conduct impact studies on climate change, it is necessary to adjust climate simulation outputs from the control period to match the statistical characteristics of observed data at gauging stations (Soriano et al., 2019). Biases between climate simulation output and observed data can arise due to poor conceptualization, discretization, and spatial averaging within grid cells (Christensen et al., 2008). The ERA5 dataset

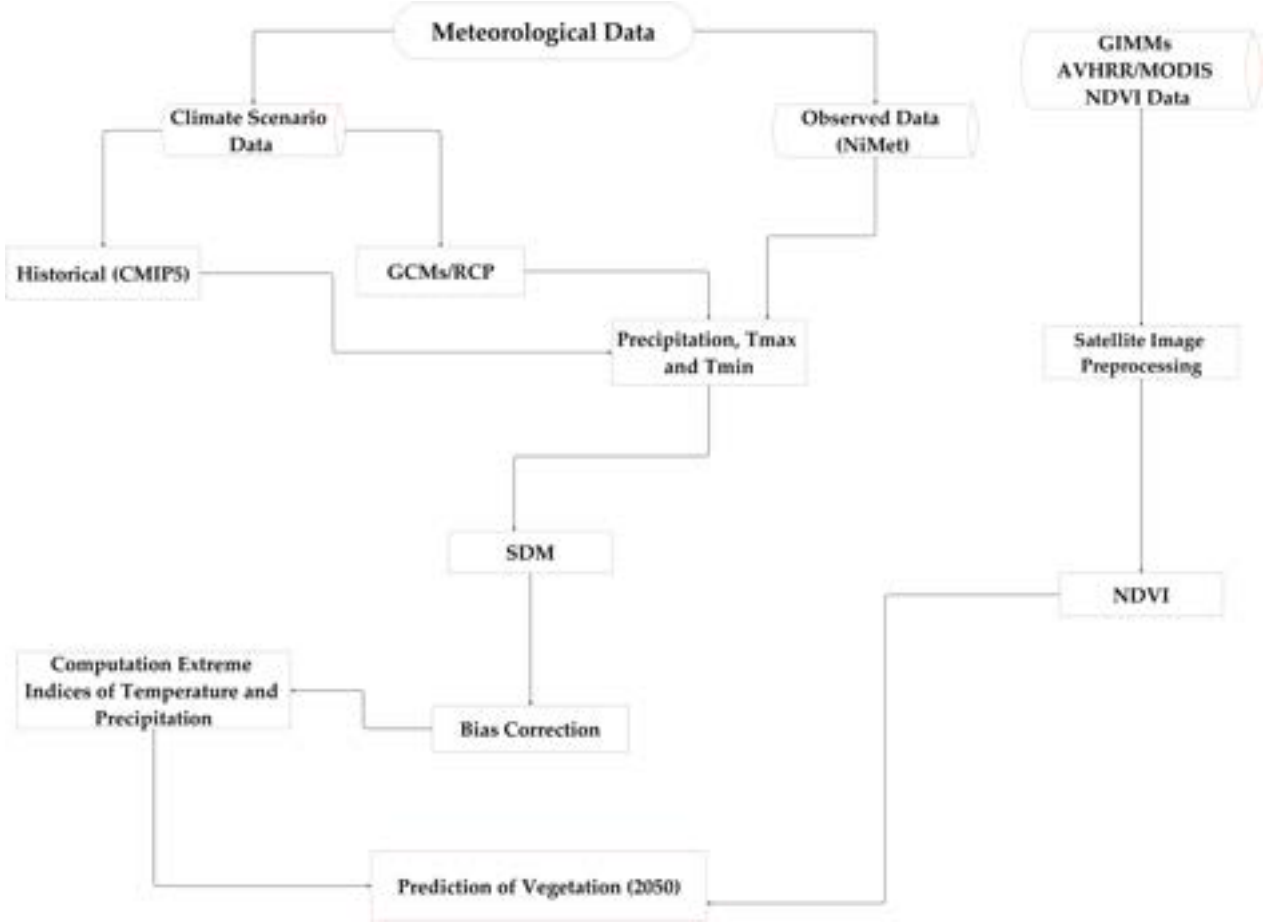

Fig. 2. Summary of the Methodology Flow Chart.

covering 1980–2022 was adjusted using a multivariate bias correction based on the N-dimension probability (MBCn) method to address this. This adjustment aimed to provide a geographically comprehensive and optimal representation of climate research at the spatial level rather than relying solely on discrete observed data with high temporal accuracy. Each climate station within the dataset underwent downscaling and bias-correcting using MBCn, which accounted for temporal, spatial, and variable biases in the dataset.

The MBCn method, developed by Cannon (2018), employs a multivariate quantile delta mapping (QDM) approach combined with random orthogonal function applied to both model and observation data. The N-dimensional probability density function is rotated to correct it using QDM and then rotated back. This sequence of iterations involving multivariate and univariate transformations continues until the best match between the corrected and observed multivariate distributions is achieved. In this study, a hundred iterations were conducted. The MBCn method, being a multivariate quantile delta mapping (QDM), reassigns all characteristics of the observed distribution to the simulations. The MBCn package in the R software was utilized for this purpose. For a more detailed theoretical description, please refer to Adeyeri et al. (2020b), Cannon (2018), and Meyer et al. (2019).

Computation of Extreme Indices.

The 27 core indices proposed by the Expert Team on Climate Change Detection and Indices (ETCCDI) were used to choose the indices for this study, shown in Table 4. Folland et al. (2001) and Yosef et al. (2021) recommended the 27 core indices. The indices were calculated using Climpact2-master, an R-based software program created by ETCCDI. These data were used to compute extreme indices of temperature and precipitation as well as drought indices (Standard Precipitation Index and Standardized Precipitation Evapotranspiration Index). SPEI and SPI are commonly utilized in more than 70 nations because they are normalized or standardized to location and time (Tefera et al., 2019). SPEI and SPI measure how wet or dry a region is over time in various periods (Liu et al., 2021). Precipitation levels are anticipated to deviate from the normal distribution because daily data may contain a large number of zero values (Livada and Assimakopoulos, 2007). Variations in rainfall, and maximum and minimum temperature on seasonal, decadal, and inter-annual trends were identified. A subset of the quarterly values for the typical three-month seasons, i.e., March–April–May (MAM), June–July–August (JJA), September–October–November (SON), and December–January–February (DJF), for the annual values of climate variables and associated extreme indices, using meteorological data collected from NiMet. (See Fig. 2 for the methodology flow chart).

Daily maximum and minimum temperatures were averaged to determine the monthly and annual variables. To determine the total yearly precipitation, the monthly precipitation was added together. We utilized Mann Kendall trend analysis to evaluate trends in NDVI, precipitation, and maximum and minimum temperature. We used correlation and linear regression on layers of annual NDVI extreme temperature and precipitation indices to investigate how climate variability affects vegetation change in the study area.

Mann Kendall Test.

The time series data analysis can be conducted using parametric and non-parametric tests, focusing exclusively on consistent data. Parametric trend tests have higher statistical power but require independent and normally distributed data. In contrast, nonparametric tests are advantageous for analyzing hydro-meteorological time series as they do not rely on assumptions about data distribution (Hossein et al., 2019). The nonparametric time series analysis, i.e. Mann Kendall, is used in this study. However, to use Mann Kendall rank method, it is essential to consider autocorrelation to check for randomness and periodicity in the series. A positive autocorrelation may result in an overestimation, and a negative autocorrelation may result in an underestimation of a trend. The presence of autocorrelation in the residuals of the studied variable will be assessed by examining the autocorrelation function (ACF) and partial autocorrelation function (PACF) at a significance level of $\alpha = 0.05$.

Next, the Mann-Kendall (M−K) rank correlation test was employed to ascertain the trend's direction and significance. The significance of the trend will be tested at 5 % levels. To perform the M−K test, the difference between the earlier and the latter is measured values (yj – yi) where j > i are computed. Values of +1, 0 and −1 are assigned H_0 the positive and negative differences, respectively, as ranks. The test statistics are then computed as integer values.

The non-parametric Mann-Kendall test was employed to identify monotonic trends in daily rainfall, minimum and maximum temperature, and extreme indices of temperature and precipitation time series (Mann, 1945; Kendall, 1975). Due to its robustness against outliers and its ability to handle non-normally distributed data, the Mann-Kendall statistical test has become widely used in evaluating the significance of trends in hydro-meteorological time series (Scherrer et al., 2016; Zobel et al., 2018; Salihu, 2021). The following are the statistics (S) of the Mann-Kendall test:

$$S = \sum_{i=1}^{n-1} \sum_{j=i+1}^{n} sign\left(X_j - X_i\right) \tag{1}$$

where 'n' represents the number of data points,'X'_j*and*'X'_i represent annual values in years 'j' and 'i' respectively (where 'j' is greater than 1), and 'Sign (X_j*and*X_i)' is calculated using a specific equationbelow

$$Sign\left(X_j - X_i\right) = \begin{cases} -1 for\left(X_j - X_i\right) & < 0 \\ 0 for\left(X_j - X_i\right) & = 0 \\ +1 for\left(X_j - X_i\right) & > 0 \end{cases} \tag{2}$$

The term "Sign (Xj – Xi)" refers to the individual sign capability, which can take on values of 1, 0, or −1. A positive value (S) indicates an upward or ever-increasing trend, while a negative value suggests a downward trend. However, a statistical analysis is still necessary to determine the validity or significance of the observed phenomenon. Kendall (1975) describes the test procedure using the normal approximation test. The test assumes that the dataset does not include a significant number of tied or closely related values. The variance (S) is calculated using the following equation:

$$Var(S) = \frac{1}{18}\left[n(n-1)(2n+5) - \sum_{p=1}^{g} t_p\left(t_p - 1\right)\left(2t_p + 5\right)\right] \tag{3}$$

Where:

- n is the number of data points,
- g represents the count of zero differences between compared values,
- tp denotes the number of data points in the p^{th} group.

A standardized measure of test statistics (Zs) is computed using the given equation:

$$Z_s = \begin{cases} \dfrac{S-1}{\sqrt{Var(S)}}, & if S < 0 \\ 0 & if S = 0 \\ \dfrac{S+1}{\sqrt{Var(S)}}, & if S > 0 \end{cases} \tag{4}$$

A positive value of the test statistics indicates increasing trends, while a negative value reflects decreasing trends. A value of 0 suggests no discernible trend. The testing of trends was conducted at a specific significance level. When the absolute value of the test statistic is greater than the critical value obtained from the standard normal distribution table, the null hypothesis is rejected, indicating the presence of a significant trend in the time series. This study employed a significance level of $\alpha = 0.05$. Oguntunde et al. (2012) and Daramola et al. (2017) have confirmed that at the 5 % significance level, the null hypothesis of no trend is rejected when the absolute value of the test statistic is greater

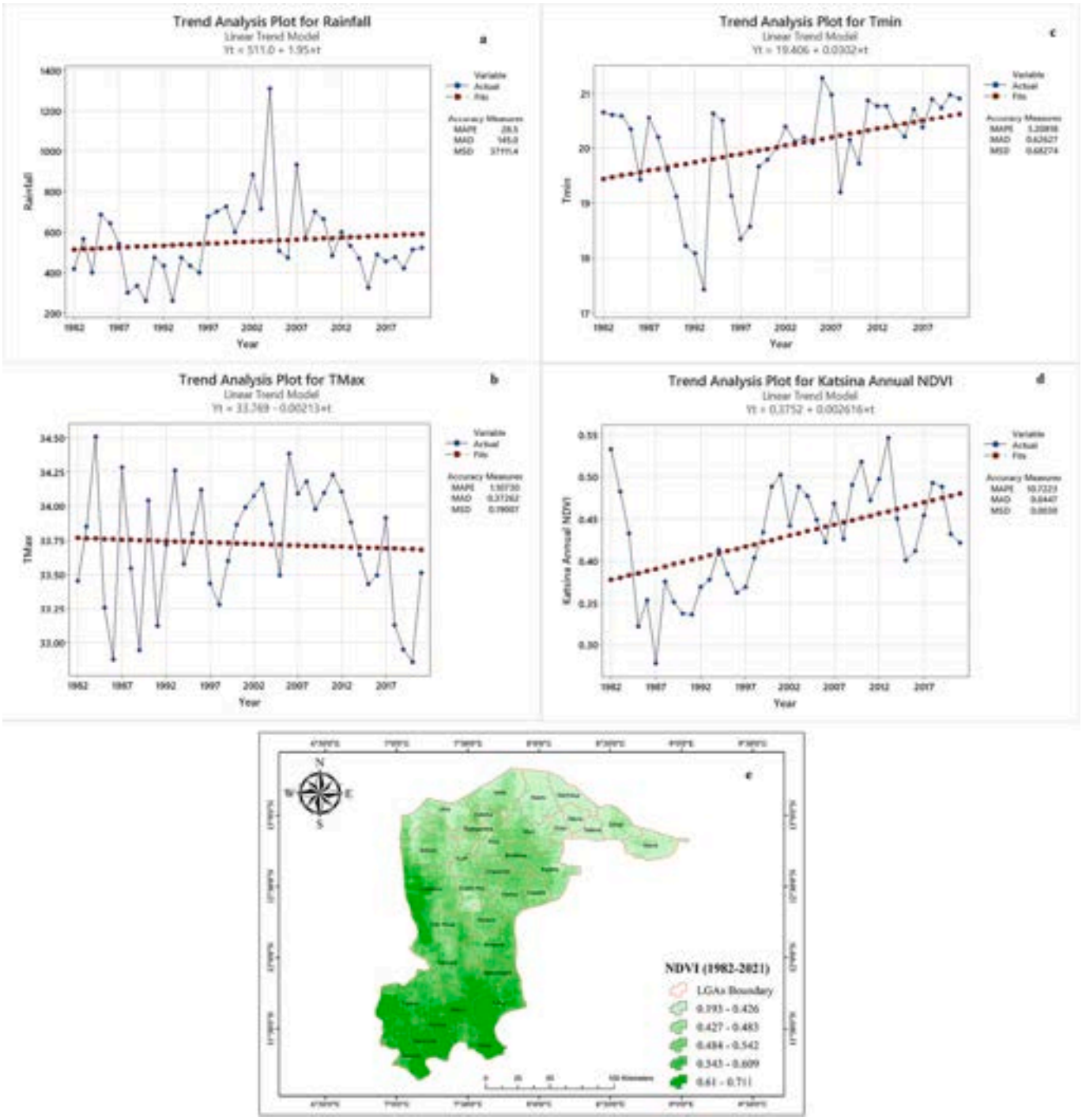

Fig. 3. Interannual trend and pattern of climatic variables and vegetation of Katsina from 1982 to 2021 (a. Rainfall trend, b. Tmax trend, c. Tmin trend, d. NDVI trend and e. spatial distribution of NDVI.

than 1.96. Consequently, they conclude that there is a significant trend present in the time series.

Simple linear regression is a commonly utilized model for identifying linear trends and is widely employed as one of the primary approaches in trend analysis. However, the assumption of residual normality is necessary for this method (McBean and Motiee, 2008). The Sen (2014) slope estimator is a powerful tool for developing linear relationships unaffected by data errors and outliers. It is determined as the mean of all pair-wise slopes in the dataset. The individual slope (mij) is estimated using the following equation:

$$m_{ij} = \frac{Y_j - Y_i}{j - i} \tag{5}$$

The Sen's slope is calculated as the mean of the slopes estimated using the Sen Estimator. These slopes are computed for a time series with n values, where i ranges from 1 to n − 1 and j ranges from 2 to n. The data values at time j and time i are represented by Yj and Yi, respectively. In total, N = n(n-2) such slopes are used to determine the Sen's slope.

$$m_{\left[\frac{N+1}{2}\right]} \; ifnisodd \tag{6}$$

$$m = \frac{1}{2}\left(m_{\frac{N}{2}+m_{\left[\frac{N+2}{2}\right]}}\right) ifniseven$$

A positive Sen's slope indicates an upward trend, whereas a negative Sen's slope suggests a downward trend.

Correlation.

Correlation coefficients measure the strength of association between two continuous variables. The strength or degree of association between two sets of time series is a measure of the impact of one upon the other, in this case, the impact of climate variability on the water resources variables. The higher correlation coefficient values mean a higher degree or level of impact. The potential effects of climate change on the vegetation, relationship coefficients between NDVI and precipitation, Tmax, and Tmin in the Katsina state were calculated according to the following formula:

$$R_{xy} = \frac{\sum_{i=1}^{n}(x_i-\overline{x})(y_i-\overline{y})}{\sqrt{\sum_{i=1}^{n}(x_i-\overline{x})^2}\sqrt{\sum_{i=1}^{n}(y_i-\overline{y})^2}}$$

Linear Regression.

The following equation is commonly used to represent the linear regression model:

$$Y = M \times X + C \tag{7}$$

In the linear regression model, the dependent variable (NDVI) is represented by Y. The independent variable (Climatic variables) is denoted by X. The line slope (mm/year) is represented by m, and the intercept constant coefficient is represented by C. The model's coefficients (m and C) are estimated using the commonly employed Least-Squares method, which is widely used in practice. The sign of the slope determines the direction of the trend variable: it indicates an increase if the sign is positive and a decrease if the sign is negative. The seasonal, annual, and decadal data trend analysis in Katsina state was conducted using Sen's slope estimator and the Mann-Kendall test with XLSTAT software. Additionally, regression analysis was employed to establish a linear relationship over time based on the observed rainfall data.

To assess the significance of the trend, it is essential to calculate the slope's standard error (SE) and determine the degree of freedom (n − 2) using the series for analysis. The S_E is calculated using:

$$S_E = \frac{\sqrt{\left[\frac{\sum(y_i-\widehat{y_i})}{(n-2)}\right]}}{\sqrt{\left[\sum(x_i-\overline{x})^2\right]}}$$

In the context of regression analysis, the observed dependent variable is represented by yi, the observed independent variable is represented by xi, the mean of the independent variable is denoted by ×, and the estimated value of the dependent variable is represented by y. To evaluate the presence of a significant trend, the ratios of the slope (ß) and S_E are computed using the following formula:

$$t = \frac{\beta}{S_E}$$

To assess its significance, the computed ratio (t) is compared to the values on a t-table at a significance level corresponding to the degrees of freedom (n − 2) (Anandhi et al. 2013). Herein, a trend is considered statistically significant if it demonstrates significance at the 5 % level.

Test for step changes.

The climatic data underwent a homogeneity test to assess the presence of sudden or abrupt changes. The Pettitt test (Pettitt, 1980) was utilized to determine the homogeneity of the time series datasets. The Pettitt test is a statistical method that relies on ranks to detect significant changes in the mean of time series data when the specific timing of the change is uncertain. The Pettitt test demonstrates resilience to changes in the distributional form of time series data. It is known for its superior statistical power compared to alternative tests such as the Wilcoxon-Mann-Whitney test, CUSUM, and cumulative deviations (Kundzewicz and Robson, 2004). The test statistic is represented by the equation below:

$$U_{t,N} = U_{t,-1,N} + \sum_{j=1}^{N} sgn(x_t - x_j) for t = 2, \cdots, N$$

The test statistic is computed by counting the occurrences where a member of the first sample surpasses a member of the second sample. In the Pettitt test, the null hypothesis assumes the absence of a change point. The test statistic *Kt* and the associated probabilities are used for assessing the significance of the test, and they are given as follows:

$$k_t = Max_{1\le t\ge N}\left|U_{t,N}\right|$$

$$p \cong 2\exp\left\{-6(k_t)^2/\left(N^3+N^2\right)\right\}$$

Here, p represents the chosen level of significance. If the change point is deemed significant, the time series is divided into two sections at the identified change point, *t*.

A gamma distribution is fitted to rainfall data, and the SPI is calculated. A negative SPI value indicates a drought situation, while a positive value indicates a period of wet conditions. The WMO recommends the

Table 5
Characteristic and Non-Parametric Trend of Extreme Temperature and Precipitation Indices, Rainfall, Maximum, and Minimum Temperature Distribution.

Variable	Mean	CV	Z	S	p-value
Rainfall	1.56	0.36	0.22	129	0.07
TMax	33.79	0.01	0.16	97	0.17
Tmin	19.92	0.05	0.17	99	0.16
CSDI	2.65	1.9			
CDD	203.79	0.17	−0.06	–32	0.64
CWD	3.68	0.32	0.26	122	0.05
DTR	14.09	0.09	0.02	11	0.87
GSL	365.24	0	0.02	8	0.87
PRCPTOT	560.27	0.37	0.18	101	0.13
R10mm	18.85	0.34	0.08	43	0.52
R20mm	9.59	0.57	0.2	109	0.1
R95p	119.34	1.09	0.11	59	0.38
R99p	34.88	2.04	0.13	49	0.35
Rx1day	53.73	0.45	0.11	61	0.37
Rx5day	85.19	0.36	0.26	144	0.03
SDII	13.06	0.3	0.01	7	0.92
SU	357.09	0.02	0.26	143	0.03
TN10p	8.55	0.82	−0.09	−52	0.44
TN90p	8.65	0.69	0.15	84	0.21
TNn	8.75	0.18	0.12	62	0.35
TNx	29.49	0.07	−0.18	−97	0.14
TR	193.71	0.15	0.29	160	0.02
TX10p	8.98	0.27	−0.03	−16	0.81
TX90p	8.42	0.52	0.27	153	0.02
TXn	23.04	0.08	0.1	51	0.44
TXx	100.29	3.33	−0.02	−9	0.89
WSDI	2.91	1.59	0.32	131	0.02
SPEI_3 Month	−0.023	−25.084	0.049	26	0.701
SPEI_6 Month	−0.027	−27.339	0.121	64	0.332
SPEI_12 Month	−0.031	−28.516	0.205	108	0.098
SPEI_24 Month	−0.024	−38.841	0.22	116	0.075
SPI_3 Month	−0.22	−13.427	0.205	108	0.098
SPI_6 Month	0.097	7.152	0.22	116	0.075
SPI_12 Month	−0.004	−221.811	0.269	142	0.028
SPI_24 Month	−0.013	−65.536	0.299	158	0.014

Note: STD: – Standard Deviation and CV: – Coefficient of Variation CV: – Coefficient of Variation, Z: – Kendall's tau, S: – Slope.

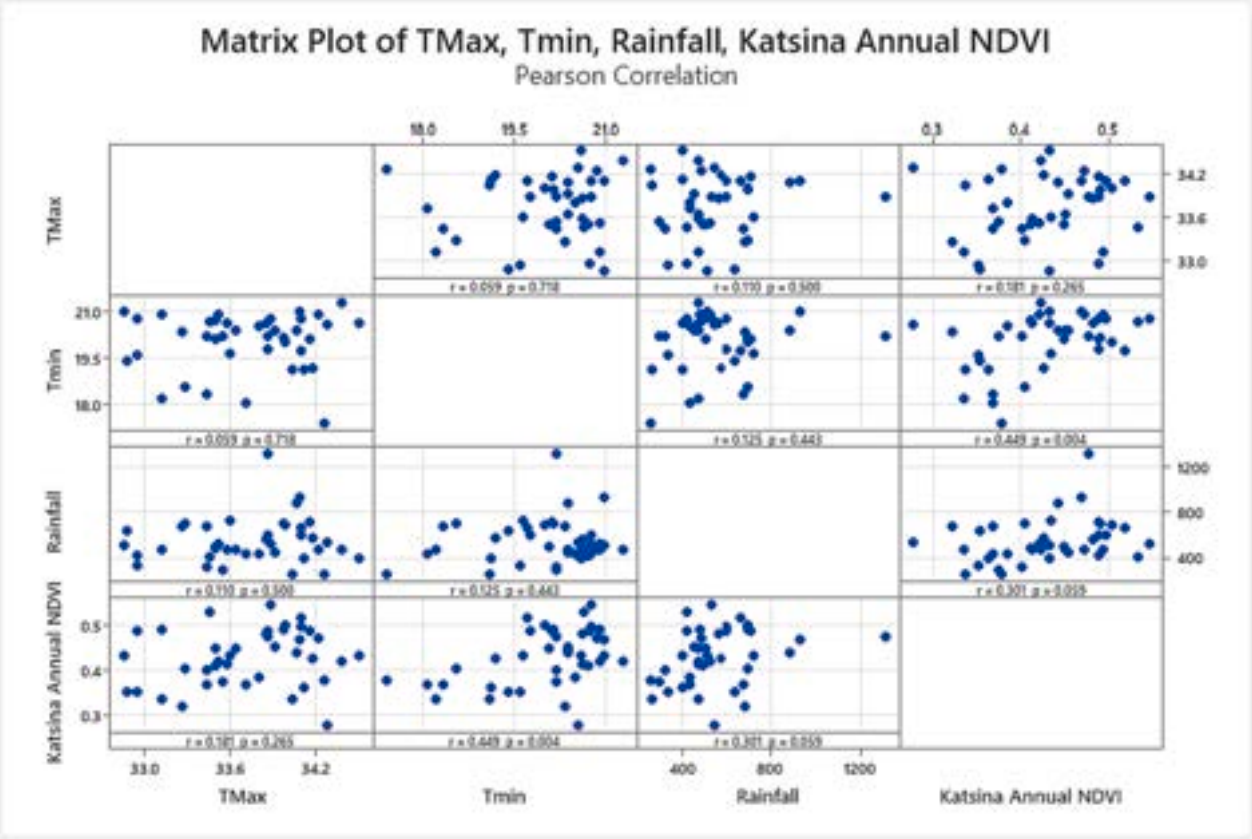

Fig. 4. Correlation analysis of the Precipitation, Tmax, and Tmin Using Observed data from NiMet (1982–2021).

SPI. Also, SPEI is based on the same assumptions as SPI, where climatic water balance was considered.

3. Results

3.1. Inter-annual variability of extreme indices and climatic variables

Fig. 3e shows the spatial distribution of vegetation across Katsina state from 1982 to 2021 with NDVI values ranging from 0.193 to 0.711. Jibia, Kankia, and Mashi Local Government Areas have lower NDVI values of 0.193–0.426. A range of 0.193 to 0.426 suggests moderate vegetation density from Fig. 3. It could indicate areas with sparse vegetation, possibly due to limited water availability, soil quality, or land use practices. 0.484–0.542 NDVI value was found around Musawa, Malumfashi, and some parts of Bindawa LGAs. These areas show moderately higher NDVI values compared to the previous range. NDVI values ranging from 0.484 to 0.542 indicate denser vegetation cover with better water availability, soil conditions, or land management. Bakori, Danja, and Funtua LGAs have the highest NDVI values of 0.61–0.711, suggesting dense and vigorous vegetation due to favorable environmental factors. Fig. 3e provides insights into vegetation health, with higher NDVI values indicating denser vegetation.

Fig. 3a to 3d illustrate the long-term interannual trends of rainfall, maximum temperature (Tmax), minimum temperature (Tmin), and MODIS (NDVI) in Katsina state from 1982 to 2021. The data presented in these Figures indicate inconsistency in the interannual variability of these variables over time. Fig. 3a showcases the interannual trend of rainfall distribution across Katsina state.

Specifically, Fig. 3a shows higher rainfall in 2004 and lower levels in 1990 and 1993. Similarly, Fig. 3b reveals that Tmax was higher in 1984 and lower in 1986 and 2020. Additionally, Fig. 3c portrays that Tmin was higher in 2006 and lower in 1993. Lastly, Fig. 3d demonstrates that NDVI was higher in 2013 and lower in 1987. These findings suggest temporal fluctuations in the interannual variability of these variables. Furthermore, the Figures indicate positive trends in rainfall, Tmin, and NDVI, while Tmax displayed a negative trend between 1982 and 2021.

Characteristics and non-parametric trends of Rainfall, maximum and minimum temperature, and the twenty-four (24) selected extreme indices of temperatures and rainfall based on ETCCDI/ET-SCI Indices are presented in Table 5. The result revealed that PRCPTOT and GSL indices had the highest and the second-highest mean values. Moreover, CSDI and rainfall had the first and the second lowest mean values. TMax, SU, Tmin, TNx, TXn, and DTR had low variability, while TX10p, SDII, CWD, R10mm, Rainfall, Rx5day, and PRCPTOT had moderate variability in the state. Rx1day, TX90p, R20mm, TN90p, TN10p, R95p, WSDI, CSDI, R99p, and TXx showed high variability in the study.

SDII, DTR, GSL, R10mm, TXn, SPEI, R95p, Rx1day, TNn, R99p, TN90p, Tmax, Tmin, PRCPTOT, R20mm, Rainfall, CWD, Rx5day, SU, TX90p, TR, WSDI, SPEI (3 month, 6 month, 12 month, and 24 months), SPI (3 month, 6 month, 12 month, and 24 month) had a positive trend with the positive Sen's slope while TNx, TN10p, CDD, TX10p, and TXx had a negative trend with negative Sen's slope. In addition, only SU, TR, TX90p, CWD, Rx5day, WSDI SPI_12month, and SPI_24months indices show a significant trend at 0.05 level. The result revealed an overall increasing trend in NDVI in Katsina from 1982 to 2021, with a large interannual variation, which increases and decreases in vegetation, sometimes lasting several years (Fig. 3d).

3.2. Impact of climate variability on vegetation

Fig. 4 investigates the relationship between precipitation, maximum temperature (Tmax), and minimum temperature (Tmin) in Katsina state using observed data from NiMet between 1982 and 2021. The results indicate that the correlation coefficient (r) between

Table 6
Impact of climate variability on vegetation changes.

Variables	Coefficient	Standard error	t	Pr > |t|	Lower bound (95 %)	Upper bound (95 %)
Constant	−6.592	17.340	−0.380	0.710	−44.372	31.187
TMax	0.064	0.035	1.859	0.088	−0.011	0.140
Tmin	0.014	0.019	0.753	0.466	−0.026	0.054
Rainfall	−0.015	0.027	−0.578	0.574	−0.074	0.043
CSDI	0.006	0.004	1.519	0.155	−0.002	0.014
CDD	0.000	0.000	0.720	0.485	−0.001	0.001
CWD	0.011	0.014	0.785	0.448	−0.019	0.040
DTR	−0.113	0.100	−1.128	0.281	−0.331	0.105
GSL	0.023	0.047	0.490	0.633	−0.080	0.126
PRCPTOT	−0.001	0.001	−1.514	0.156	−0.002	0.000
R10mm	0.015	0.007	2.029	0.065	−0.001	0.031
R20mm	0.011	0.009	1.217	0.247	−0.009	0.032
R95p	0.000	0.000	0.643	0.532	−0.001	0.001
R99p	0.000	0.000	0.279	0.785	−0.001	0.001
Rx1day	0.001	0.001	0.560	0.585	−0.002	0.004
Rx5day	0.000	0.001	0.262	0.798	−0.002	0.003
SDII	−0.006	0.010	−0.569	0.580	−0.029	0.017
SU	−0.001	0.004	−0.287	0.779	−0.011	0.008
TN10p	0.014	0.009	1.591	0.138	−0.005	0.033
TN90p	0.000	0.006	0.022	0.983	−0.012	0.013
TNn	−0.019	0.012	−1.599	0.136	−0.045	0.007
TNx	0.016	0.010	1.646	0.126	−0.005	0.037
TR	−0.001	0.001	−0.414	0.686	−0.004	0.003
TX10p	−0.018	0.009	−2.086	0.059	−0.037	0.001
TX90p	0.010	0.008	1.275	0.227	−0.007	0.027
TXn	0.012	0.012	0.981	0.346	−0.015	0.039
TXx	−0.059	0.024	−2.447	0.031	−0.112	−0.006
WSDI	0.005	0.003	1.601	0.135	−0.002	0.011

precipitation and Tmax is 0.059, with a p-value of 0.718, suggesting a weak and non-significant correlation between these variables. Similarly, the correlation between precipitation and Tmin is 0.110, with a p-value of 0.500, indicating a weak and non-significant correlation. The correlation between Tmax and Tmin is 0.181 with a p-value of 0.265, suggesting a weak positive correlation between these variables, which is also not statistically significant. Interestingly, the correlation between Tmax and rainfall is 0.500 with a p-value of 0.001, indicating a moderate positive correlation between these variables. This finding suggests that when Tmax increases, rainfall tends to increase as well, and vice versa. The correlation between Tmax and NDVI is 0.181 with a p-value of 0.265, indicating a weak positive correlation between these variables, which is not statistically significant. These findings suggest that while there is a moderate positive correlation between Tmax and rainfall, there is no significant relationship between Tmax, Tmin, and NDVI in Katsina state.

However, the correlation coefficient (r) of 0.059 and p-value of 0.718 between precipitation and Tmax suggests no significant correlation between the two variables. This means that changes in Tmax do not necessarily cause corresponding changes in precipitation levels and vice versa. The correlation coefficients of 0.125 and 0.443 and p-values of Tmin and rainfall suggest a weak to moderate positive correlation between Tmin and rainfall. This implies that an increase in Tmin could lead to an increase in rainfall and vice versa. The correlation coefficient of 0.449 and p-value of 0.004 between Tmin and NDVI suggest a strong positive correlation between the two variables. This implies that an increase in Tmin is associated with an increase in NDVI, which could indicate improved vegetation growth in the region. This means that correlation analysis results suggest that Tmin has a stronger association with rainfall and NDVI than Tmax does with these variables.

More so, the correlation between NDVI and Tmax is weak, with an r-value of 0.181 and a non-significant p-value of 0.265. This indicates no strong relationship exists between vegetation growth and maximum temperature in Katsina state. The correlation between NDVI and Tmin is moderately strong, with an r-value of 0.449 and a very low p-value of 0.004. This suggests a positive correlation between vegetation growth and minimum temperature. This could be because higher temperatures during the nighttime lead to increased evapotranspiration, which can promote vegetation growth. The correlation between NDVI and rainfall is moderate, with an r-value of 0.301 and a p-value of 0.059, which is marginally significant. This suggests a positive correlation between vegetation growth and precipitation, although this relationship is not particularly strong. In summary, the correlation analysis indicates a weak relationship between NDVI and Tmax, a moderately strong positive relationship between NDVI and Tmin, and a moderate positive relationship between NDVI and rainfall in Katsina state. These findings provide insights into the complex relationships between climate variables and vegetation growth in the region.

This study employed a comprehensive linear regression analysis model to investigate the influence of climate variability on vegetation. The model incorporated multiple independent variables, such as precipitation, maximum temperature (Tmax), minimum temperature (Tmin), extreme temperature, and precipitation indices. The dependent variable utilized in this analysis was the Normalized Difference Vegetation Index (NDVI), obtained from MODIS (Table 6). The results show a negative regression coefficient of Rainfall, DTR, PRCPTOT, SDII, SU, TNn, TR, TX10p, and TXx variables, meaning an inverse relationship exists between the dependent and the explanatory/independent variables. This implies that an increase in these variables had decreased the vegetation density change. However, the variables were statistically not significant in this study at <0.01 level. Fig. 4 depicts the correlation analysis of precipitation, maximum temperature (Tmax), and minimum temperature (Tmin).

Furthermore, there is a strong negative correlation between precipitation and extreme precipitation indices, indicating that as precipitation increases, the likelihood of extreme cold events increases. Finally, there is a weak negative correlation between precipitation and extreme temperature indices, which suggests that higher precipitation is associated with a lower likelihood of extreme temperature events.

The Equation of the model is as follows;

$$\begin{aligned}\textit{Predicted NDVI} = {} & -6.59241 + 0.06449 * \text{TMax} + 0.01398 * \text{Tmin} - 0.01549 * \text{Rainfall} \\ & + 0.00567 * \text{CSDI} + 0.00035 * \text{CDD} + 0.01073 * \text{CWD} - 0.11291 * \text{DTR} \\ & + 0.02321 * \text{GSL} - 0.00060 * \text{PRCPTOT} + 0.01494 * \text{R10mm} + 0.01148 \\ & * \text{R20mm} + 0.00026 * \text{R95p} + 0.00014 * \text{R99p} + 0.00080 * \text{Rx1day} + 0.00034 \\ & * \text{Rx5day} - 0.00596 * \text{SDII} - 0.00123 * \text{SU} + 0.01383 * \text{TN10p} + 0.00012 \\ & * \text{TN90p} - 0.01904 * \text{TNn} + 0.01610 * \text{TNx} - 0.00062 * \text{TR} - 0.01827 * \text{TX10p} \\ & + 0.01014 * \text{TX90p} + 0.01200 * \text{TXn} - 0.05930 * \text{TXx} + 0.00484 * \text{WSDI}\end{aligned}$$

.

More frequent extreme events that affect vegetation cover result from climate change. Tmax and Tmin had a detrimental effect on the vegetation, leading to temperature indices having a beneficial impact. The positive regression coefficient indicates a direct correlation between the variables, whereas the negative value reveals an inverse correlation between the research area's indexes and NDVI. DTR, PRCPTOT, and SDII had negative regression coefficients, which shows an inverse relationship between the variables. Tmax and Tmin had positive regression coefficients, meaning a direct relationship exists between independent variables and the vegetation (NDVI). Although, none of the explanatory variables was statistically significant at a 0.05 level of confidence. NDVI, rainfall, maximum and minimum temperature, and extreme indices were strongly correlated in the study area.

However, a strong negative correlation exists between precipitation and Tmin, indicating that higher precipitation is associated with lower Tmin. This can be attributed to the cooling effect of rain. Additionally, there is a weak negative correlation between Tmax and extreme temperature indices, which suggests that higher Tmax is associated with a lower likelihood of extreme temperature events.

3.3. Predictions of temperature, rainfall, and extreme indices

3.3.1. Inter-annual variability of the predicted rainfall, maximum/minimum temperature

The Inter-annual variability of the predicted rainfall, Tmax, and Tmin in Katsina state was assessed from 2022 – 2050. Fig. 5 reveals the study area's predicted rainfall, minimum and maximum temperature.

Trend analysis results presented in Fig. 5(a – i) provide information about the projected changes in rainfall, maximum and minimum temperature under different Representative Concentration Pathways (RCPs). Fig. 5g shows the rainfall under RCP8.5 with a positive trend and the highest precipitation in 2050. It suggests that, according to the model projections, precipitation levels are expected to increase over time. Additionally, it shows that the highest precipitation values are projected to occur in the year 2050. Fig. 5h presents the Tmax under RCP8.5 with a positive trend and highest in 2032. This Figure represents the maximum temperature (Tmax) trends under the RCP8.5 scenario. It indicates a positive trend; this implies that temperatures are projected to increase over time. The highest Tmax values are expected to occur in the year 2032. Fig. 5i indicates the RCP8.5 positive trend and highest in

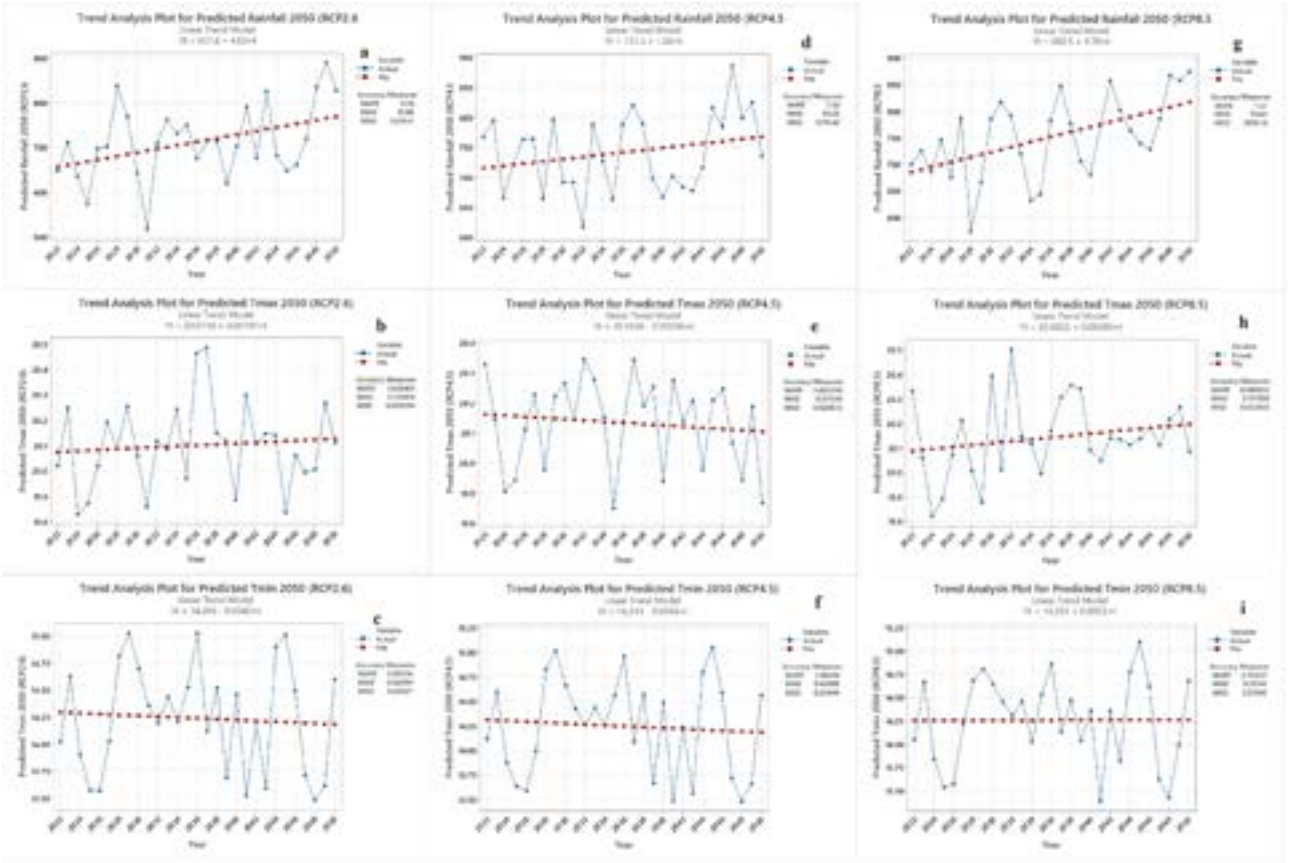

Fig. 5. Interannual Variability of the predicted climatic variables (a, b, and c are Rainfall, Tmax, and Tmin under RCP26; d, e, and f are Rainfall, Tmax, and Tmin under RCP45 while g,h, and I are Rainfall, Tmax and Tmin under RCP28.5 respectively).

Table 7
Characteristics of Interannual Predicted Extreme Temperature and Precipitation Indices Distribution.

Emission	Indices	Mean	STD	CV	Z	S	P-value
RCP2.5	CDD	2.1	4.36	2.08	−0.55	−152	0
	CSDI	0	0		−0.09	−34	0.53
	CWD	242.25	588.05	2.43	0.06	29	0.64
	DTR	13.44	9.49	0.71	−0.05	−16	0.73
	GSL	365.26	0.44	0	0.29	135	0.02
	PRCPTOT	4333.85	1808.04	0.42	0.25	116	0.05
	R10mm	284.65	139.09	0.49	0.34	156	0.01
	R20mm	39.65	21.58	0.54	0.24	111	0.06
	R95p	502.22	322.57	0.64	0.16	74	0.21
	R99p	114.7	104.1	0.91	0.28	129	0.03
	Rx1day	34	12.37	0.36	0.33	155	0.01
	RX5day	150.56	60.6	0.4	0.27	127	0.03
	SDII	12.1	4.5	0.37	0.03	15	0.81
	SU	28.77	6.89	0.24			
	Tn10p	7.08	3.53	0.5	−0.57	−267	< 0.0001
	Tn90p	10.67	4.08	0.38	−0.02	−7	0.92
	TNn	2.33	4.75	2.04	−0.57	−157	0
	Tnx	13.57	6.56	0.48	−0.33	−152	0.01
	TR	44.97	91.84	2.04	−0.56	−154	0
	Tx10p	9.83	4.37	0.44	−0.02	−11	0.87
	Tx90p	9.77	5.56	0.57	−0.02	−7	0.92
	Txn	11.47	0.99	0.09	0.23	103	0.08
	TXx	29.56	7.06	0.24	−0.34	−156	0.01
	WSDI	5.16	10.05	1.95	−0.14	−49	0.32
RCP4.5	CDD	11.68	5.24	0.45	−0.14	−61	0.3
	CSDI	5.35	10.1	1.89	0.12	42	0.41
	CWD	31.42	10.59	0.34	0.04	17	0.78
	DTR	−5.88	0.5	−0.08	−0.08	−35	0.57
	GSL	365.26	0.44	0	−0.05	−16	0.73
	PRCPTOT	696.72	64.96	0.09	0.19	87	0.15
	R10mm	0.74	0.76	1.03	−0.16	−60	0.28
	R20mm	0	0		0.06	29	0.64
	R95p	86.97	30.51	0.35	−0.1	−44	0.46
	R99p	20.82	13.69	0.66	−0.08	−35	0.56
	Rx1day	10.2	1.59	0.16	0.13	62	0.3
	RX5day	29.87	4	0.13	0.21	97	0.1
	SDII	2.95	0.14	0.05	−0.11	−49	0.41
	SU	30.06	9.19	0.31			
	Tn10p	9.97	4.52	0.45	−0.14	−65	0.28
	Tn90p	9.97	3.36	0.34	−0.25	−115	0.05
	TNn	11.85	0.46	0.04	−0.29	−130	0.03
	Tnx	26.53	0.36	0.01	0.01	6	0.93
	TR	235.06	5.52	0.02	0.07	31	0.61
	Tx10p	8.55	5.01	0.59	−0.09	−44	0.46
	Tx90p	8.36	5.46	0.65	−0.17	−81	0.18
	Txn	9.59	0.44	0.05	−0.02	−7	0.91
	TXx	40.34	5.15	0.13	−0.06	−29	0.63
	WSDI	6.48	12.92	1.99	0.06	21	0.68
RCP2.6	CDD	13.19	4.28	0.32	−0.25	−114	0.05
	CSDI	3.42	5.96	1.74	0.02	8	0.88
	CWD	30.29	13.51	0.45	0.25	115	0.05
	DTR	−5.85	0.5	−0.09	−0.12	−57	0.34
	GSL	365.26	0.44	0	−0.05	−16	0.73
	PRCPTOT	665.03	84.81	0.13	0.26	119	0.04
	R10mm	0.65	1.03	1.6	0.12	43	0.42
	R20mm	0	0		0.02	7	0.92
	R95p	82.35	34.32	0.42	0	1	1
	R99p	21.41	22.55	1.05	−0.08	−37	0.54
	Rx1day	9.95	1.56	0.16	0	2	0.99
	RX5day	30.23	3.91	0.13	0.15	71	0.24
	SDII	2.91	0.16	0.06	−0.16	−72	0.23
	SU	30.68	9.87	0.32			
	Tn10p	9.95	3.39	0.34	−0.14	−65	0.28
	Tn90p	9.97	4.38	0.44	−0.18	−83	0.17
	TNn	11.95	0.46	0.04	−0.23	−104	0.08
	Tnx	26.48	0.34	0.01	−0.07	–33	0.58
	TR	235.77	6.24	0.03	0.16	74	0.21
	Tx10p	8.79	5.61	0.64	−0.11	−50	0.4
	Tx90p	8.63	6.24	0.72	−0.18	−83	0.17
	Txn	9.64	0.39	0.04	0.13	50	0.37
	TXx	40.67	4.92	0.12	−0.11	−52	0.39
	WSDI	6.03	14.59	2.42	−0.13	−42	0.38

Note: STD: – Standard Deviation and CV: – Coefficient of Variation, Z: – Kendall's tau, S: – Slope.

Table 8
Characteristics of Interannual Predicted Drought Indices Distribution.

Indices	Emission	Time	Mean	STD	Z	S	P-value
SPI	RCP2.6	3 Months	0.01	0.67	0.09	43	0.48
		6 Months	0.02	0.81	0.05	21	0.74
		12 Months	0.03	0.88	0.03	15	0.81
		24 Months	0.05	0.9	−0.04	−17	0.79
	RCP4.5	3 Months	0.01	0.61	0.1	45	0.46
		6 Months	0.01	0.72	0.09	41	0.5
		12 Months	0.02	0.8	0.1	46	0.44
		24 Months	−0.01	0.87	0.16	73	0.22
	RCP28.5	3 Months	−0.01	0.41	0.06	29	0.64
		6 Months	−0.02	0.58	0.05	23	0.71
		12 Months	−0.06	0.92	−0.03	−13	0.84
		24 Months	0.11	0.92	−0.26	−119	0.04
SPEI	RCP2.6	3 Months	0.01	0.63	0.1	45	0.46
		6 Months	0.03	0.77	0.05	23	0.71
		12 Months	0.05	0.88	0.06	27	0.66
		24 Months	0.03	0.89	0.09	40	0.51
	RCP4.5	3 Months	0	0.54	0.16	75	0.21
		6 Months	0.01	0.69	0.13	61	0.31
		12 Months	0.03	0.89	0.15	69	0.25
		24 Months	0.04	0.92	0.19	89	0.14
	RCP8.5	3 Months	−0.07	0.47	0.06	28	0.65
		6 Months	−0.05	0.6	0.07	33	0.59
		12 Months	−0.08	0.95	0	−1	1
		24 Months	0.02	0.95	−0.2	−93	0.12

Note: STD: – Standard Deviation and CV: – Coefficient of Variation CV: – Coefficient of Variation, Z: – Kendall's tau, S: – Slope.

2045. The Figure shows a positive trend under the RCP8.5 scenario. It could refer to either precipitation or temperature, depending on the details provided in the source. The highest values are projected to occur in the year 2045.

Fig. 5d reveals the rainfall RCP4.5 positive trend and the highest precipitation in 2048. It suggests increasing precipitation levels over time, with the highest values projected to occur in 2048. Fig. 5e shows the RCP4.5 Tmax negative trend and highest in 2032. In this Figure, the negative trend in Tmax under the RCP4.5 scenario indicates that temperatures are projected to decrease over time. The highest Tmax values are expected to occur in the year 2032. Fig. 5f RCP4.5 Tmin negative trend and highest in 2045 represents the minimum temperature (Tmin) trends under the RCP4.5 scenario. The negative trend indicates a projected decrease in Tmin over time. The highest Tmin values are expected to occur in the year 2045.

Fig. 5a shows the rainfall RCP2.6 positive trend and highest precipitation in 2049. It suggests increasing precipitation levels over time, with the highest values projected to occur in 2049. Fig. 5b shows the RCP2.6 Tmax positive trend and highest in 2037. This Figure indicates a positive trend in Tmax under the RCP2.6 scenario, suggesting increasing temperatures over time. The highest Tmax values are projected to occur in the year 2037. Fig. 5c shows the RCP2.6 negative trend and highest in 2036. The negative trend in this Figure, under the RCP2.6 scenario, could refer to precipitation or temperature, depending on the context of the source. The highest values are projected to occur in the year 2036.

These trend analysis results provide insights into the projected changes in precipitation and temperature under different climate scenarios. They help understand future climate conditions and can be valuable for climate impact assessments, adaptation planning, and policy-making.

3.3.2. *Inter-annual variability of the predicted extreme indices*

Table 7 shows the time series of the predicted extreme temperature and precipitation indices averaged over the study area from 2020 to 2050. The predicted temperature and precipitation indices under RCP2.6 revealed that DTR, GSL, Tnx, TR, TNn, Txn, and SDII indices had low variability. Moderate variability was observed in TXx, PRCPTOT, RX5day, Rx1day, CDD, SU, and Tn10p, while high variability was in R95p, Tn90p, CWD, Tx10p, Tx90p, R99p, R10mm, CSDI, WSDI, and R20mm between the indices under study in Katsina state. The results also show that the Mann-Kendall Z for the predicted temperature and precipitation indices in Katsina station under RCP 2.6 (low Emission) based on CMIP5 models revealed that CDD, TNn, Tn90p, Tx90p, SDII, Tn10p, WSDI, DTR, Tx10p, TXx, R99p, Tnx, and GSL indices had a negative trend with negative Sen's slope. In contrast to R95p, Rx1day, CSDI, R20mm, R10mm, Txn, RX5day, TR, CWD, and PRCPTOT indices with a positive trend and the positive Sen's slope (S). However, only CDD, CWD, and PRCPTOT among the 24 indices show a significant trend at 0.05 level.

The characteristics of the predicted extreme temperature and precipitation indices averaged over the study area during 2020 – 2050 under the influence of medium emission (RCP4.5) are presented in Table 7. The analysis also revealed that TNn, Tn90p, Tx90p, R10mm, CDD, Tn10p, SDII, and R95p had negative Z values, with high variability among the indices. DTR, GSL, Tnx, TR, TNn, SDII, Txn, and PRCPTOT indices have low variability with positive trends throughout the study period, respectively. Moderate variability was observed in RX5day, TXx, Rx1day, SU, CWD, Tn90p, and R95p indices. The Mann-Kendall Z for Tx10p, DTR, R99p, TXx, GSL, and Txn indices show a negative trend with a negative Sen's slope. In contrast, Tnx, CWD, R20mm, WSDI, TR, CSDI, Rx1day, PRCPTOT, and RX5day indices had a positive trend with the positive Sen's slope (S). In addition, Tn90p and TNn indices reveal a significant trend at a 0.05 level.

Results for the extreme indices under high emission (RCP8.5) are presented in Table 7. The predicted temperature and precipitation indices under RCP8.5 generally reveal high variability among the studied indices. GSL and Txn indices had low variability. Moderate variability was observed in SU, TXx, Rx1day, SDII, and Tn90p. In contrast, high variability was in RX5day, PRCPTOT, Tx10p, Tnx, R10mm, Tn10p, R20mm, Tx90p, R95p, DTR, R99p, WSDI, TNn, TR, CDD, CWD, and CSDI between the indices from the coefficient of variability result. Decomposing time series analysis of the precipitation (PRCT), maximum and minimum temperature (Tmax and Tmin) climatic variables under RCP2.6, RCP4.5, and RCP8.5 were presented in the app. endix. Table 7 presents the characteristics of the interannual predicted distribution of extreme temperature and precipitation indices.

Mann-Kendall (Z) for the predicted temperature and precipitation extreme indices under RCP 8.5 (high emission) based on CMIP5 models shows that Tn10p, TNn, TR, CDD, TXx, Tnx, WSDI, CSDI, DTR, Tn90p, Tx10p, and Tx90p indices had a negative trend with negative Sen's slope, while SDII, CWD, R95p, Txn, R20mm, PRCPTOT, RX5day, R99p, GSL, Rx1day, R10mm indices had a positive trend with the positive Sen's slope (S) (Table 7). In addition, TXx, TR, Tnx, TNn, Tn10p, Rx5day, Rx1day, R99p, R10mm, PRCPTOT, GSL, and CDD indices show a significant trend at 0.05 level (Table 7). Table 8 outlines the characteristics of the interannual predicted distribution of drought indices.

Table 8 revealed the characteristics of the predicted drought indices (SPI) and (SPEI) under RCP2.6 (Low emission), RCP4.5 (medium emission), and RCP8.5 (high emission) for the 3 month, 6 month, 12 month, and 24 month. The results show that the study area might experience a mild drought based on the prediction under RCP4.5 and RCP8.5 according to the SPI/SPEI drought category classification scale adapted from Mohammed et al. (2022). The SPI indices of 3,6, 12, and 24 months under RCP2.6 had a negative trend with a negative Sen's slope, while SPI under RCP4.5 and RCP8.5 had a positive trend with a positive Sen's slope (S) (Table 8). In addition, only 24-month SPI under RCP8.5 shows a significant trend at 0.05 level. The mean value shows that 24-month SPI under medium emission together with 3-, 6-, and 12-months SPI under high emission indicate drought conditions while SPI (3, 6, 12, and 24 months) under low emission and SPI (3, 6, and 12 month) under medium emission reveals wet condition across the study area (Table 8). Although, there is a significant trend in the predicted 24-month SPI under high emissions.

There were no significant drought indices (SPEI) trends for any of the

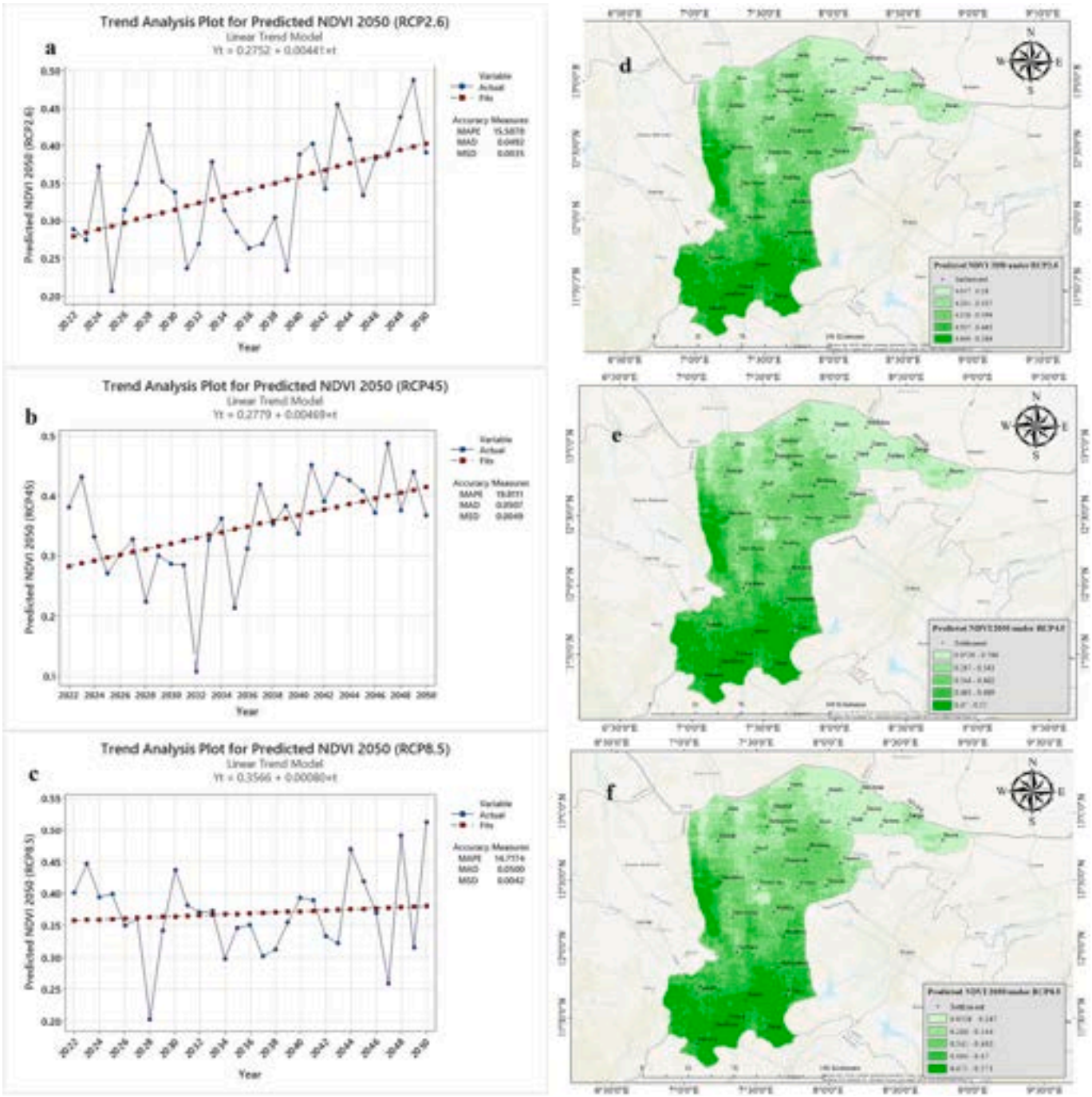

Fig. 6. Predicted trend and spatial distribution of NDVI under the Influences of Extreme Temperature and Precipitation Indices (RCP2.6, 4.5 and 8.5).

three scenarios for the 2020–2050 period at a 0.05 confidence level. However, the trend of the drought indices (SPEI) based on CMIP5 models for the RCP2.6 (low emission), RCP4.5 (medium emission), and RCP8.5 (high emission) scenarios in the future period (2020–2050) revealed that all the predicted SPEI of 3, 6, 12 and 24 months under low, moderate, and high emission shows a positive tendency with positive Sen's slope. The mean value indicates that SPEI under high emission in 3, 6, and 12 months indicated a drought condition with a negative mean. In contrast, Low, medium, and high emissions (24 months) indicated wet conditions across the study area within the study periods.

4. Discussion

Table 5 reveals the characteristics and non-parametric trend of extreme temperature and precipitation indices and the climatic elements (rainfall, maximum and minimum temperatures) over an interannual period. SU, TR, TX90p, CWD, Rx5day, WSDI SPI_12month, and SPI_24month indices increased significantly. Vegetation has also increased in the study area. In the same way, vegetation maintains its natural regeneration. Although at the regional and global level, the study's results confirm those of previous studies on greening and regreening vegetation (de Jong et al., 2011; Anyamba et al., 2014; Dubovyk et al., 2015).

Using the changes in indices of daily temperature and precipitation

extremes, Abdussalam (2015) pointed out that "Katsina state is vulnerable to climate extremes due to its physical and socioeconomic characteristics, like poverty, desertification, environmental disturbances, high population growth rates, and extreme climates" with significant, increasing trends found in the annual minimum of daily maximum and minimum temperature, the annual maximum of daily maximum and minimum temperature, the number of summer nights, and the number of days where daily temperature has exceeded its 90th percentile. In this study area, disease burden and extreme weather events are projected to disproportionately affect the region, which has been identified as a climate change hotspot (Abdussalam, 2015).

To better understand the impact of climate variability over the long term, it is crucial to monitor vegetation change in relation to climatic parameters (rainfall, Tmax, and Tmin) and extreme temperature and precipitation indices. Table 6 shows the influence of extreme indices, temperature, and rainfall on vegetation distribution in the study area. The results reveal that none of the explanatory variables was statistically significant. NDVI, precipitation, and maximum and minimum temperature extreme indices were strongly correlated in the study area. The findings of this study align with previous global studies on extreme temperature and precipitation, such as Donat et al. (2013) and Yin et al. (2015). Donat et al. (2013) demonstrated a direct relationship between the Diurnal Temperature Range (DTR) and vegetation (NDVI). Similarly, this study reveals a strong correlation between NDVI and climatic indices.

This correlation has also been observed in previous studies conducted by Fensholt et al. (2012), Dardel et al. (2014), and Anyamba et al. (2014). The NDVI is negatively correlated with temperature in savannas, as Adepoju et al. (2019) demonstrate that the pattern of vegetation cover will continue to change (increase/decrease) under rising temperatures and rainfall, with increasing trends related to rainfall and other factors and decreasing trends due to rising in temperature and other related factors, particularly in drier regions. The results also align with a previous study that found a negative relationship between temperature and vegetation (Zahraddeen et al., 2019). According to the study conducted in Nigeria by Ekundayo et al. (2021), rainfall plays a significant role in determining vegetation patterns, accounting for 60 % of the observed variation in vegetation.

The annual rainfall variability in all emission predictions (RCP28.5, RCP4.5, and RCP2.6) showed increasing trends from 2022 to 2050 (Fig. 5a, d and g), respectively. There is an increasing trend in the high and low emission forecasts but a decreasing trend in the medium emission (RCP4.5) forecasts based on the maximum temperature (Fig. 5b, 5e and h). On the other hand, low and medium emission forecasts showed a decrease in minimum temperatures, while high emission shows increasing trends (Fig. 5c, f and i). Mouhamed et al. (2013) revealed a comparable finding that throughout the West African Sahel, all temperature indices point to a general warming trend since 1960. As for rainfall-related indices, although there was a general tendency of decreased annual total rainfall, the observed trends are less uniform than the ones in temperatures. Some indices indicate that extreme rainfall events have become more frequent during the last decade. However, the observed warming trend means a higher demand for domestic energy consumption for cooling, a higher evaporation rate from water bodies and irrigated crops, and a lower performance of crops and livestock. On the other hand, an increased frequency of extreme rainfall events, such as heavy downpours and long dry or wet spells, means more fragile infrastructure and production systems.

However, the study's findings support previous research by Buba et al. (2017), Ifabiyi and Ojoye (2013), and Odekunle et al. (2008) on rainfall trends in the Sudano-Sahelian ecological region of Nigeria. These studies collectively found that the rise in annual rainfall in the Sudano-Sahelian environmental region of Nigeria can be attributed primarily to a significant increase in rainfall during the wet season. This observation serves as an indicator of climate change occurring within the region.

A significant trend is observed for CDD, CWD, and PRCPTOT among the 24 indices under low emission (Table 7), and Tn90p and TNn indices at a 0.05 level of significance under medium emission (Table 7), and TXx, TR, Tnx, TNn, Tn10p, Rx5day, Rx1day, R99p, R10mm, PRCPTOT, GSL, and CDD indices (Table 7). Previous studies have shown similar trends in extreme temperatures and precipitation indices (Zhou et al., 2016; Yin and Sun, 2018; Li et al., 2021).

Over the study period, there was no significant trend in SPI_3, SPI_6, and SPI_12 months and SPEI_3, SPEI_6, SPEI_12, and SPEI_24 months of the drought indices. Only SPI_24 months under high emissions had a significant trend. However, the descriptive analysis for the predicted drought indices shows a tendency. This is because 24-month SPI under medium emission and 3, 6, or monthly SPI under high emission indicate drought conditions as they have negative mean values. At the same time, there was a tendency for SPI (3, 6, 12, and 24 months) under low emission and SPI (3, 6, and 12 months) under medium emission for wet conditions across the study area (Table 8). As it had negative averages, the SPEI under RCP28.5 in 3, 6, and 12 months revealed a tendency for drought conditions. The study period was marked by moist conditions over the area, as indicated by low, medium, and high emissions (24 months). These findings concur with those of Mohammed et al. (2022).

Trend analysis results from the Minitab statistical software of NDVI under three RCPs are presented in Fig. 6a, Fig. 5b, and Fig. 6c) while Fig. 6d, e and f) reveal the spatial variability of vegetation (NDVI) predictions based on precipitation, Tmax, Tmin and extreme indices of temperature and precipitation indices for low, medium, and high emissions levels. This study predicts a mixed trend in future vegetation changes in the area, with increasing and decreasing patterns. Some areas show an upward trend, indicating an expected increase in vegetation, while others exhibit a downward trend, suggesting a decrease (Fig. 6a – c). This aligns with the findings of Usman et al. (2013), which reveal that Katsina state has the highest coefficient of variation in temperature for the entire time series; thus, based on the threshold value of the coefficient of variation of rainfall reported by Shepherd et al. (1987). By implication, this suggests that areas around Katsina experienced more changes in vegetation NDVI and possibly their ecosystems.

Climate models were used to estimate the changes in climate variables and extreme temperature and precipitation indices from 2022 to 2050. Rainfall, Tmin, and Tmax have increased in all three RCP scenarios compared to the baseline period. In the scenarios of RCP2.6, RCP4.5, and RCP8.5, the annual climate variables and indices are projected to increase throughout the future period. Relationships between predictors and predictands are often non-stationary. To avoid non-stationarity, it is imperative to choose the appropriate predictor from several large-scale geographical predictors (Salvati et al., 2019). This is a crucial issue in SDSM modeling. This was accomplished using different correlation tests and trial-and-error methods to screen the variables in the SDSM and select the appropriate predictors. As a result of environmental issues, desertification is likely to continue encroaching on state borders.

The rise in Katsina state's annual total rainfall aligns with Lebel and Ali's (2009) research and may be attributed to the recovery of the Sahelian rainfall (Adeyeri et al., 2019; Jajere et al., 2022). Additionally, the study area displays a significant upward trend in very wet and extremely wet days, consistent with Touré Halimatou et al. (2017) and Sarr's (2012) discoveries of amplified extreme rainfall incidents in the Sahel. It's important to note that, despite the growing frequency of extreme rainfall events, there is a surge in consecutive dry days and a decrease in consecutive wet days.

The increasing trend of greenhouse gas emissions, such as carbon dioxide and methane, in the atmosphere can contribute to climate warming and lead to the growing trend for climate indices in Katsina State. More so, changes in land use patterns, such as deforestation and urbanization, can affect the region's surface temperature and precipitation patterns. These changes can also alter the surface albedo, further amplifying the warming effect. Understanding the mechanisms behind

the increasing trend of climate indices in Katsina State can provide insights into the underlying causes and help develop appropriate adaptation and mitigation strategies. It is important to note that the mechanisms contributing to the trend may vary depending on the specific climate indices being analyzed.

According to James et al. (2018), Katsina state is experiencing an increasing trend in maximum temperature and precipitation and a decreasing trend in minimum temperature. This trend has made the area highly sensitive to aridity, which poses a direct negative impact on both the livelihood and ecosystem of the state. The rise in maximum temperature, coupled with climate variability, has heightened the degree of sensitivity to aridity in Katsina, and human activities such as logging, bush burning, and conversion of forested areas to agricultural land are contributing factors to this environmental problem. As aridity continues to increase throughout the state, it will significantly negatively impact vegetation cover, water availability, rainfall distribution patterns, ecosystem health, and biodiversity.

The study area exhibited a more prominent trend in the temperature indices analyzed, which contrasts with previous studies conducted in other parts of Africa. Saley et al. (2019) noted a warming trend in the Sahel from 1960 to 2010. Similarly, Abatan et al. (2016) reported warming trends in Nigeria from 1971 to 2012, with the greatest warming occurring in southern Nigeria. These findings align with our results, although Ferrelli et al. (2019) and Henchiri et al. (2021) identified the most substantial warming trends in stations along the coast.

A novel approach for assessing the vegetation ecosystem of drylands with remote sensing data and statistical analysis in relation to extreme indices is presented in this study. However, the accuracy of the estimated NDVI values may be impacted by uncertainties in the vegetation index, insufficient qualitative and quantitative data, and the influence of extreme precipitation and temperature events. Verifying the simulated NDVI values using more precise remote sensing data and human observations is crucial to ensure reliable results. This verification process can be achieved through high-precision remote sensing mapping and ground-level verification of vegetation in the study area.

5. Limitations and uncertainties

This study presents a comprehensive evaluation of the impact of daily temperature and extreme precipitation indices on vegetation dynamics in Katsina State using SDM. However, it is important to acknowledge certain limitations and uncertainties within our analysis. Firstly, the NDVI data utilized in this study may be influenced by factors such as cloud cover, solar altitude angle, and atmospheric conditions. The relatively low spatial resolution of the vegetation index data could potentially limit its ability to accurately reflect the actual vegetation status within the 250 m resolution, introducing uncertainties into our results. Moreover, the uneven distribution of meteorological stations poses another limitation. The scarcity of climatic stations in certain areas may result in less precise temperature and precipitation data. This imbalance in data availability could be a possible reason for the lower correlations observed between NDVI and precipitation/temperature. Therefore, it is crucial to incorporate more accurate climate and NDVI data to validate the findings of this study.

Additionally, the uncertainty associated with remote sensing data can impact the accuracy of vegetation distribution information, leading to uncertainties in vegetation mapping (Wang et al., 2021; Shen et al., 2022). To further analyze vegetation distribution changes, it is recommended to incorporate additional vegetation indices such as EVI, TVDI, RWSI, and SAVI, among others. For a more accurate understanding of the influence of climate change on vegetation dynamics, future research should explore the effects of other environmental factors on vegetation in Katsina State. While this study solely focuses on the influence of daily temperature and precipitation extreme indices, other climatic factors, including wind, solar radiation, and relative humidity, can also impact vegetation cover. Hence, future studies need to investigate the effects of these factors on NDVI and vegetation dynamics.

The validation of the prediction model for vegetation dynamics in Katsina State, Nigeria, under extreme temperature and precipitation indices, utilized a time series validation method. This approach assessed the model's performance by comparing its predictions to observed data. The lagged cross-validation technique was employed to address the presence of temporal dependencies. The model's usefulness in monitoring and controlling vegetation in response to climate extremes was determined based on the validation results and expert feedback. It was concluded that the model's accuracy and usefulness were significant.

In summary, while this study provides valuable insights into the influence of daily temperature and extreme precipitation indices on vegetation dynamics in Katsina State, several limitations and areas for further research should be considered. By addressing these limitations and expanding the scope of analysis, we can better understand the relationship between climate factors and vegetation dynamics in the region.

6. Conclusion

This study uses NDVI data from the Advanced Very High-Resolution Radiometer (AVHRR) sensor and Moderate Resolution Imaging Spectroradiometer (MODIS) over 40 years (1982–2021) to track vegetation change dynamics in Nigeria's savannah for 40 years (1982–2021). Landsat imagery, climate data (precipitation, Tmax, Tmin), and socioeconomic data were also used. A significant trend pattern change was observed in climate variables, extreme weather indices, and NDVI. Separate analyses were conducted on NDVI, extreme indices of temperature and precipitation, and climatic variables. NDVI, climate variables, and indices were then analyzed using regression analysis to determine the degree of impact. Climate variability within the study area strongly correlates with vegetation changes. However, between 2020 and 2050, rainfall indices are projected to increase and have a positive impact on vegetation under the three emission scenarios RCP2.6, RCP4.5, and RCP28.5, while TXx and TXn show negative impacts on vegetation under low, medium, and high emission scenarios across the study periods. However, the drought indices (SPEI and SPI) predicted under RCP4.5 and RCP8.5 indicate a mild drought may occur, which would negatively affect vegetation in the study area. Because vegetation degradation is believed to be spreading in the extreme northern regions of the study area, an early warning system for the dangers associated with desertification and other environmental problems is recommended. To predict the condition of vegetation regarding its driving forces across the study area, further research should use geospatial simulation models like the Analytical Hierarchy Process (AHP) and Technique for Order Preference by Similarity to Ideal Solution (TOPSIS). The study uses a statistical downscaling model to estimate the daily temperature and precipitation extremes. This model assumes that the relationships between the large-scale climate variables and the local weather variables are linear and stationary, which may not always be the case. Although, the study does not consider other important factors such as soil quality, land use, and human activities. This may limit the accuracy and reliability of the study's conclusions.

CRediT authorship contribution statement

Mohammad Hadi Ahmad: Conceptualization, Methodology, Software, Formal analysis, Investigation, Resources, Data curation, Writing – original draft. **Ahmed Abubakar:** Conceptualization, Software, Formal analysis, Investigation, Data curation, Writing – original draft. **Mohd Yusoff Ishak:** Validation, Project administration. **Samir Shehu Danhassan:** Visualization. **Zhang Jiahua:** Visualization. **Juha M. Alatalo:** Validation, Writing – review & editing, Supervision.

Declaration of Competing Interest

The authors declare that they have no known competing financial interests or personal relationships that could have appeared to influence the work reported in this paper.

Data availability

Data will be made available on request.

Acknowledgment

The authors thank two anonymous reviewers for their constructive comments that improved the manuscript. Open Access funding was provided by the Qatar National Library.

Appendix A. Supplementary data

Supplementary data to this article can be found online at https://doi.org/10.1016/j.ecolind.2023.110979.

References

Abiodun, B.J., Adeyewa, Z.D., Oguntunde, P.G., Salami, A.T., Ajayi, V.O., 2012. Modeling the impacts of reforestation on future climate in West Africa. Theoretical and Applied Climatology 110 (1–2), 77–96. https://doi.org/10.1007/s00704-012-0614-1.

Adamu, M.B., Adamu, H., Ade, S.M., Akeh, G.I., 2020. Household Energy Consumption in Nigeria: A Review on the Applicability of the Energy Ladder Model. Journal of Applied Sciences and Environmental Management 24 (2), 237–244. https://doi.org/10.4314/jasem.v24i2.7.

Adejuwon, J.O., Dada, E., 2021. Temporal analysis of drought characteristics in the tropical semi-arid zone of Nigeria. Scientific African 14, 1–11. https://doi.org/10.1016/j.sciaf.2021.e01016.

Adepoju, K., Adelabu, S., Fashae, O., 2019. Vegetation Response to Recent Trends in Climate and Landuse Dynamics in a Typical Humid and Dry Tropical Region under Global Change. Advances in Meteorology 2019, 1–15.

Adeyeri, O.E., Lawin, A.E., Laux, P., Ishola, K.A., Ige, S.O., 2019. Analysis of climate extreme indices over the Komadugu-Yobe basin, Lake Chad region: Past and future occurrences. Weather and Climate Extremes 23, 100194.

Akpu, B., Tanko, A., Jeb, D., Dogo, B., 2017. Geospatial Analysis of Urban Expansion and Its Impact on Vegetation Cover in Kaduna Metropolis, Nigeria. Asian Journal of Environment & Ecology 3 (2), 1–11. https://doi.org/10.9734/ajee/2017/31149.

Alaanuloluwa Ikhuoso, O., Adegbeye, M.J., Elghandour, M.M.Y., Mellado, M., Al-Dobaib, S.N., Salem, A.Z.M., 2020. Climate change and agriculture: The competition for limited resources amidst crop farmers-livestock herding conflict in Nigeria - A review. Journal of Cleaner Production 272, 1–9. https://doi.org/10.1016/j.jclepro.2020.123104.

Alemaka, J., Sawa, B.A., Yusuf, R.O., 2021. Effect of Temperature on the Incidence of Cerebro-Spinal Meningitis and Its Management in Funtua Local Government Area, Katsina State. Nigeria. *J. Appl. Sci. Environ. Manage.* 25 (7), 1311–1316.

Anav, A., Mariotti, A., 2011. Sensitivity of natural vegetation to climate change in the Euro-Mediterranean area. Climate Research 46 (3), 277–292. https://doi.org/10.3354/cr00993.

Anyamba, A., Small, J.L., Tucker, C.J., Pak, E.W., 2014. Thirty-two Years of Sahelian Zone Growing Season Non-Stationary NDVI3g Patterns. Remote Sensing 6 (4), 3101–3122. https://doi.org/10.3390/rs6043101.

Biasutti, M., 2019. Rainfall trends in the African Sahel: Characteristics, processes, and causes. Wiley Interdisciplinary Reviews: Climate Change 10 (4), 1–22. https://doi.org/10.1002/wcc.591.

Bouriaud, O., Leban, J.M., Bert, D., Deleuze, C., 2005. Intra-annual variations in climate influence growth and wood density of Norway spruce. Tree Physiology 25 (6), 651–660. https://doi.org/10.1093/treephys/25.6.651.

Brooks, N., 2004. Drought in the African Sahel: Long term perspectives and future prospects. Tyndall Centre Working Paper No. 61. 1-31.

Buba, L.F., Kura, N.U., Dakagan, J.B., 2017. Spatiotemporal trend analysis of changing rainfall characteristics in Guinea Savanna of Nigeria. Modeling Earth Systems and Environment 3 (3), 1081–1090. https://doi.org/10.1007/s40808-017-0356-2.

Buytaert, W., Cuesta-Camacho, F., Tobón, C., 2011. Potential impacts of climate change on the environmental services of humid tropical alpine regions. Global Ecology and Biogeography 20 (1), 19–33. https://doi.org/10.1111/j.1466-8238.2010.00585.x.

Cao, S., Ma, H., Yuan, W., Wang, X., 2014. Interaction of ecological and social factors affects vegetation recovery in China. Biological Conservation 180, 270–277. https://doi.org/10.1016/j.biocon.2014.10.009.

Cao, Q., Yu, D., Georgescu, M., Han, Z., Wu, J., 2015. Impacts of land use and land cover change on regional climate: A case study in the agro-pastoral transitional zone of China. Environmental Research Letters 10 (12), 1–12. https://doi.org/10.1088/1748-9326/10/12/124025.

Carré, M., Azzoug, M., Zaharias, P., Camara, A., Cheddadi, R., Chevalier, M., Fiorillo, D., Gaye, A.T., Janicot, S., Khodri, M., Lazar, A., Lazareth, C.E., Mignot, J., Mitma García, N., Patris, N., Perrot, O., Wade, M., 2019. Modern drought conditions in western Sahel unprecedented in the past 1600 years. Climate Dynamics 52 (3–4), 1949–1964. https://doi.org/10.1007/s00382-018-4311-3.

Dagnachew, M., Dagnachew, M., Kebede, A., Moges, A., Abebe, A., 2020. Effects of Climate Variability on Normalized Difference Vegetation Index (NDVI) in the Gojeb River Catchment, Omo-Gibe Basin, Ethiopia. Advances in Meteorology 2020, 1–16. https://doi.org/10.1155/2020/8263246.

Dardel, C., Kergoat, L., Hiernaux, P., Mougin, E., Grippa, M., Tucker, C.J., 2014. Re-greening Sahel: 30 years of remote sensing data and field observations (Mali, Niger). Remote Sensing of Environment 140, 350–364. https://doi.org/10.1016/j.rse.2013.09.011.

de Jong, R., de Bruin, S., de Wit, A., Schaepman, M.E., Dent, D.L., 2011. Analysis of monotonic greening and browning trends from global NDVI time-series. Remote Sensing of Environment 115 (2), 692–702. https://doi.org/10.1016/j.rse.2010.10.011.

!"count(.//sb:host[1]//child::*//sb:date)">Dogonyaro, J.B., Abaje, I.B., Bello, Y., . Impacts of Climatic Parameters on Cereal Crops in Katsina State, Nigeria. Sahel Journal of Geography, Environment and Development 3 (1), 1–9.

Donat, M.G., Alexander, L.V., Yang, H., Durre, I., Vose, R., Dunn, R.J.H., Willett, K.M., Aguilar, E., Brunet, M., Caesar, J., Hewitson, B., Jack, C., Klein Tank, A.M.G., Kruger, A.C., Marengo, J., Peterson, T.C., Renom, M., Oria Rojas, C., Rusticucci, M., Salinger, J., Elrayah, A.S., Sekele, S.S., Srivastava, A.K., Trewin, B., Villarroel, C., Vincent, L.A., Zhai, P., Zhang, X., Kitching, S., 2013. Updated analyses of temperature and precipitation extreme indices since the beginning of the twentieth century: The HadEX2 dataset. Journal of Geophysical Research – Atmospheres 118 (5), 2098–2118.

Dubovyk, O., Landmann, T., Erasmus, B.F.N., Tewes, A., Schellberg, J., 2015. Monitoring vegetation dynamics with medium resolution MODIS-EVI time series at sub-regional scale in southern Africa. International Journal of Applied Earth Observation and Geoinformation 38 (1), 175–183. https://doi.org/10.1016/j.jag.2015.01.002.

Duveiller, G., Defourny, P., Desclée, B., Mayaux, P., 2008. Deforestation in Central Africa: Estimates at regional, national and landscape levels by advanced processing of systematically-distributed Landsat extracts. Remote Sensing of Environment 112 (5), 1969–1981. https://doi.org/10.1016/j.rse.2007.07.026.

Ekundayo, O.Y., Okogbue, E.C., Akinluyi, F.O., Kalumba, A.M., Orimoloye, I.R., 2021. Spatiotemporal drought assessment using vegetation health index and standardized precipitation index over Sudano-Sahelian region of Nigeria. African Geographical Review 40 (4), 412–424. https://doi.org/10.1080/19376812.2020.1841658.

Fensholt, R., Langanke, T., Rasmussen, K., Reenberg, A., Prince, S.D., Tucker, C., Scholes, R.J., Le, Q.B., Bondeau, A., Eastman, R., Epstein, H., Gaughan, A.E., Hellden, U., Mbow, C., Olsson, L., Paruelo, J., Schweitzer, C., Seaquist, J., Wessels, K., 2012. Greenness in semi-arid areas across the globe 1981–2007 - an Earth Observing Satellite based analysis of trends and drivers. Remote Sensing of Environment 121, 144–158. https://doi.org/10.1016/j.rse.2012.01.017.

Ferrelli, F., Brendel, A.S., Aliaga, V.S., Piccolo, M.C., Perillo, G.M.E., 2019. Climate regionalization and trends based on daily temperature and precipitation extremes in the south of the Pampas (Argentina). Geographical Research Letters 45 (1), 393–416. https://doi.org/10.18172/cig.3707.

Folland, C.K., Colman, A.W., Rowell, D.P., Davey, M.K., 2001. Predictability of northeast Brazil rainfall and real-time forecast skill, 1987–98. Journal of Climate 14 (9), 1937–1958. https://doi.org/10.1175/1520-0442(2001)014<1937:PONBRA>2.0.CO;2.

Galiano, L., Martínez-Vilalta, J., Lloret, F., 2010. Drought-Induced Multifactor Decline of Scots Pine in the Pyrenees and Potential Vegetation Change by the Expansion of Co-occurring Oak Species. Ecosystems 13 (7), 978–991. https://doi.org/10.1007/s10021-010-9368-8.

Giannini, A., Kaplan, A., 2019. The role of aerosols and greenhouse gases in Sahel drought and recovery. Climatic Change 152 (3–4), 449–466. https://doi.org/10.1007/s10584-018-2341-9.

Hanjra, M.A., Qureshi, M.E., 2010. Global water crisis and future food security in an era of climate change. Food Policy 35 (5), 365–377. https://doi.org/10.1016/j.foodpol.2010.05.006.

Henchiri, M., Igbawua, T., Javed, T., Bai, Y., Zhang, S., Essifi, B., Ujoh, F., Zhang, J., 2021. Meteorological drought analysis and return periods over north and west africa and linkage with el niño–southern oscillation (Enso). Remote Sensing 13 (23), 1–32. https://doi.org/10.3390/rs13234730.

Hulme, M., 2001. Climatic perspectives on Sahelian desiccation: 1973–1998. Global Environmental Change 11 (1), 19–29. https://doi.org/10.1016/S0959-3780(00)00042-X.

Ibrahim, Y.-E.-L., Abdullahi, H., 2022. Farmers perceptions and adaptation strategies to rainfall variability in northwestern Katsina State. Nigeria. *African Journal of Agricultural Research* 18 (9), 759–769. https://doi.org/10.5897/ajar2022.16135.

Ibrahim, I., Usman, M.T., Abdulkadir, A., Emigilati, M.A., 2020. Analysis of Rainfall Distribution, Temporal Trends, and Rates of Change in the Savannah Zones of Nigeria. Atmosphere - Ocean 58 (5), 351–360. https://doi.org/10.1080/07055900.2018.1502149.

Idris, S., Mahmood, M.M., James, G.K., Olojo, O.O., Isah, A.A., Mustapha, S., 2019. Land Use/Land Change Dynamics Of Katsina State, Nigeria. International Journal of Advanced Research and Publications 3 (8), 19–27. www.ijarp.org.

Ifabiyi, I.P., Ojoye, S., 2013. Rainfall Trends in the Sudano-Sahelian Ecological Zone of Nigeria. Canadian Center of Science and Education 2, 194–202.

Jajere, A.A., Sawa, A.B., Kibon, U.A., Muhammed, B.U., Babagana-Kyari, M., 2022. Spatio-Temporal Variability Analysis of Rainfall in Kumadugu-Yobe River Basin.

Nigeria. *Geosfera Indonesia* 7 (1), 18–41. https://doi.org/10.19184/geosi.v7i1.24302.
James, G.K., Jega, I.M., Halilu, A.S., Olojo, O.O., Oyewunmi, A.S., Shar, J.T., Onuoha, H., Victor, S., Mustapha, S., Shehu, I., Waziri, A.N., Mahmood, M.M., Salman, K.S., Isah, A., 2018. Assessment of Environmental Sensitivity to Desertification in Katsina State. Nigeria. *Environment and Ecology Research* 6 (6), 545–555. https://doi.org/10.13189/eer.2018.060604.
Jansson, J.K., Hofmockel, K.S., 2020. Soil microbiomes and climate change. Nature Reviews. Microbiology 18 (1), 35–46. https://doi.org/10.1038/s41579-019-0265-7.
Langat, P.K., Kumar, L., Koech, R., 2019. Monitoring river channel dynamics using remote sensing and GIS techniques. Geomorphology 325, 92–102. https://doi.org/10.1016/j.geomorph.2018.10.007.
Lebel, T., Ali, A., 2009. Recent trends in the Central and Western Sahel rainfall regime (1990–2007). Journal of Hydrology 375 (1–2), 52–64. https://doi.org/10.1016/j.jhydrol.2008.11.030.
Li, C., Zwiers, F., Zhang, X., Li, G., Sun, Y., Wehner, M., 2021. Changes in annual extremes of daily temperature and precipitation in CMIP6 models. Journal of Climate 34 (9), 3441–3460. https://doi.org/10.1175/JCLI-D-19-1013.1.
Liu, C., Yang, C., Yang, Q., Wang, J., 2021. Spatiotemporal drought analysis by the standardized precipitation index (SPI) and standardized precipitation evapotranspiration index (SPEI) in Sichuan Province. China. *Scientific Reports* 11 (1), 1–14. https://doi.org/10.1038/s41598-020-80527-3.
Livada, I., Assimakopoulos, V.D., 2007. Spatial and temporal analysis of drought in Greece using the Standardized Precipitation Index (SPI). Theoretical and Applied Climatology 89 (3–4), 143–153. https://doi.org/10.1007/s00704-005-0227-z.
Ma, S., Qiao, Y.P., Wang, L.J., Zhang, J.C., 2021. Terrain gradient variations in ecosystem services of different vegetation types in mountainous regions: Vegetation resource conservation and sustainable development. Forest Ecology and Management 482 (November 2020), 1–14. https://doi.org/10.1016/j.foreco.2020.118856.
Mehboob, M.S., Kim, Y., Lee, J., Um, M.J., Erfanian, A., Wang, G., 2020. Projection of vegetation impacts on future droughts over West Africa using a coupled RegCM-CLM-CN-DV. Climatic Change 163 (2), 653–668. https://doi.org/10.1007/s10584-020-02879-z.
Mohammed, S., Alsafadi, K., Enaruvbe, G.O., Bashir, B., Elbeltagi, A., Széles, A., Alsalman, A., Harsanyi, E., 2022. Assessing the impacts of agricultural drought (SPI/SPEI) on maize and wheat yields across Hungary. Scientific Reports 12 (1), 1–19. https://doi.org/10.1038/s41598-022-12799-w.
O'Connell, E., 2017. Towards Adaptation of Water Resource Systems to Climatic and Socio-Economic Change. Water Resources Management 31 (10), 2965–2984. https://doi.org/10.1007/s11269-017-1734-2.
Obioha, E.E., 2008. Climate Change, Population Drift and Violent Conflict over Land Resources in Northeastern Nigeria. Journal of Human Ecology 23 (4), 311–324. https://doi.org/10.1080/09709274.2008.11906084.
Obioha, E.E., 2009. Climate Variability, Environment Change and Food Security Nexus in Nigeria. Journal of Human Ecology 26 (2), 107–121. https://doi.org/10.1080/09709274.2009.11906172.
Odekunle, T.O., Andrew, O., Aremu, S.O., 2008. Towards a wetter Sudano-Sahelian ecological zone in twenty-first century Nigeria. Weather 63 (3), 66–70. https://doi.org/10.1002/wea.172.
Ogunsola, O.E., Dilau, K.A., Ayokunnu, O.D., 2022. Temperature Variability Comparison Using Mann-Kendall Test. Journal of Science and Technology 14 (1), 29–36.
Ohunakin, O.S., Adaramola, M.S., Oyewola, O.M., 2011. Wind energy evaluation for electricity generation using WECS in seven selected locations in Nigeria. Applied Energy 88 (9), 3197–3206. https://doi.org/10.1016/j.apenergy.2011.03.022.
Okon, K., 2018. Sustainability of Wood Harvesting in Tropical Rainforest of Nigeria. Eurasian Journal of Forest Science 6 (2), 44–55. https://doi.org/10.31195/ejejfs.427416.
Perugini, L., Caporaso, L., Marconi, S., Cescatti, A., Quesada, B., De Noblet-Ducoudré, N., House, J.I., Arneth, A., 2017. Biophysical effects on temperature and precipitation due to land cover change. Environmental Research Letters 12 (5), 1–13. https://doi.org/10.1088/1748-9326/aa6b3f.
Quijas, S., Schmid, B., Balvanera, P., 2010. Plant diversity enhances provision of ecosystem services: A new synthesis. Basic and Applied Ecology 11 (7), 582–593. https://doi.org/10.1016/j.baae.2010.06.009.
Saleh, H.B.A., 2020. An Assessment of Market Gardeners ' Perception of Climate Variability and its Effect on Crop Production in Katsina Urban Area, Northwestern Nigeria. Sahel Journal of Geography, Environment and Development 1 (2), 48–55.
Saley, I.A., Salack, S., Sanda, I.S., Moussa, M.S., Bonkaney, A.L., Ly, M., Fodé, M., 2019. The possible role of the Sahel Greenbelt on the occurrence of climate extremes over the West African Sahel. Atmospheric Science Letters 20 (8), 1–11. https://doi.org/10.1002/asl.927.
Salvati, L., Zambon, I., Pignatti, G., Colantoni, A., Cividino, S., Perini, L., Pontuale, G., Cecchini, M., 2019. A Time-Series Analysis of Climate Variability in. Agriculture 9 (103), 1–18.
Sarr, B., 2012. Present and future climate change in the semi-arid region of West Africa: A crucial input for practical adaptation in agriculture. Atmospheric Science Letters 13 (2), 108–112. https://doi.org/10.1002/asl.368.
Scheiter, S., Higgins, S.I., 2009. Impacts of climate change on the vegetation of Africa: An adaptive dynamic vegetation modelling approach. Global Change Biology 15 (9), 2224–2246. https://doi.org/10.1111/j.1365-2486.2008.01838.x.
Shen, X., Liu, Y., Zhang, J., Wang, Y., Ma, R., Liu, B., Lu, X., Jiang, M., 2022. Asymmetric Impacts of Diurnal Warming on Vegetation Carbon Sequestration of Marshes in the Qinghai Tibet Plateau. Global Biogeochemical Cycles 36 (7), 1–13. https://doi.org/10.1029/2022GB007396.
Sinare, H., Gordon, L.J., 2015. Ecosystem services from woody vegetation on agricultural lands in Sudano-Sahelian West Africa. Agriculture, Ecosystems & Environment 200, 186–199. https://doi.org/10.1016/j.agee.2014.11.009.
Tefera, A.S., Ayoade, J.O., Bello, N.J., 2019. Comparative analyses of SPI and SPEI as drought assessment tools in Tigray Region. Northern Ethiopia. *SN Applied Sciences* 1 (10), 1–14. https://doi.org/10.1007/s42452-019-1326-2.
Thornton, P.K., Ericksen, P.J., Herrero, M., Challinor, A.J., 2014. Climate variability and vulnerability to climate change: A review. Global Change Biology 20 (11), 3313–3328. https://doi.org/10.1111/gcb.12581.
Touré Halimatou, A., Kalifa, T., Kyei-Baffour, N., 2017. Assessment of changing trends of daily precipitation and temperature extremes in Bamako and Ségou in Mali from 1961–2014. Weather and Climate Extremes 18 (October), 8–16. https://doi.org/10.1016/j.wace.2017.09.002.
Twomlow, S., Mugabe, F.T., Mwale, M., Delve, R., Nanja, D., Carberry, P., Howden, M., 2008. Building adaptive capacity to cope with increasing vulnerability due to climatic change in Africa - A new approach. Physics and Chemistry of the Earth 33 (8–13), 780–787. https://doi.org/10.1016/j.pce.2008.06.048.
Vicente-Serrano, S.M., Beguería, S., López-Moreno, J.I., 2010. A multiscalar drought index sensitive to global warming: The standardized precipitation evapotranspiration index. Journal of Climate 23 (7), 1696–1718. https://doi.org/10.1175/2009JCLI2909.1.
Wang, Y., Shen, X., Jiang, M., Tong, S., Lu, X., 2021. Spatiotemporal change of aboveground biomass and its response to climate change in marshes of the Tibetan Plateau. International Journal of Applied Earth Observation and Geoinformation 102, 1–10. https://doi.org/10.1016/j.jag.2021.102385.
Weiskopf, S.R., Rubenstein, M.A., Crozier, L.G., Gaichas, S., Griffis, R., Halofsky, J.E., Hyde, K.J.W., Morelli, T.L., Morisette, J.T., Muñoz, R.C., Pershing, A.J., Peterson, D. L., Poudel, R., Staudinger, M.D., Sutton-Grier, A.E., Thompson, L., Vose, J., Weltzin, J.F., Whyte, K.P., 2020. Climate change effects on biodiversity, ecosystems, ecosystem services, and natural resource management in the United States. The Science of the Total Environment 733, 1–18. https://doi.org/10.1016/j.scitotenv.2020.137782.
Yin, H., Donat, M.G., Alexander, L.V., Sun, Y., 2015. Multi-dataset comparison of gridded observed temperature and precipitation extremes over China. International Journal of Climatology 35 (10), 2809–2827. https://doi.org/10.1002/joc.4174.
Yin, H., Sun, Y., 2018. Characteristics of extreme temperature and precipitation in China in 2017 based on ETCCDI indices. Advances in Climate Change Research 9 (4), 218–226. https://doi.org/10.1016/j.accre.2019.01.001.
Yosef, Y., Aguilar, E., Alpert, P., 2021. Is it possible to fit extreme climate change indices together seamlessly in the era of accelerated warming? E963 International Journal of Climatology 41 (S1), E952. https://doi.org/10.1002/joc.6740.
Zahraddeen H.Y., Babangida A., Isiyaku I.I. (2019). Diversity and distribution of benthic macroinvertebrate fauna of nasarawa reservoir in jibia , katsina state nigeria. *FUDMA Journal of Sciences (FJS)*. *3*(1). 146-151 FJS.
Zhou, B., Xu, Y., Wu, J., Dong, S., Shi, Y., 2016. Changes in temperature and precipitation extreme indices over China: Analysis of a high-resolution grid dataset. International Journal of Climatology 36 (3), 1051–1066. https://doi.org/10.1002/joc.4400.